Hindawi
International Journal of Aerospace Engineering
Volume 2022, Article ID 8385913, 18 pages
https://doi.org/10.1155/2022/8385913

Research Article

Decentralized Adaptive Fault-Tolerant Cooperative Control for Multiple UAVs with Input Saturation and State Constraints

Minrui Fu,[1] **Yiwei Xu**,[1] **Ziquan Yu**,[1] **and Youmin Zhang**[2]

[1]*College of Automation Engineering, Nanjing University of Aeronautics and Astronautics, Nanjing 211106, China*
[2]*Department of Mechanical, Industrial and Aerospace Engineering, Concordia University, Montreal, Quebec, Canada H3G 1M8*

Correspondence should be addressed to Youmin Zhang; ymzhang@encs.concordia.ca

Received 1 April 2022; Revised 26 July 2022; Accepted 29 July 2022; Published 5 October 2022

Academic Editor: Shaoming He

This paper proposes a fault-tolerant cooperative control (FTCC) scheme for multiple UAVs in a distributed communication network against input saturation, full-state constraints, actuator faults, and unknown dynamics. Firstly, by considering physical limitations, an auxiliary control signal is designed to simplify the analysis process. Secondly, to avoid the difficulty in the backstepping design caused by full-state constraints, virtual control signals are constructed to transform constrained variables, while the dynamic surface control is adopted to avoid the phenomenon of "differential explosion." Thirdly, a disturbance observer (DO) is designed to estimate the unknown uncertainty caused by parameter uncertainty and actuator fault. Moreover, a recurrent wavelet fuzzy neural network (RWFNN) is used to compensate for the estimation errors of DO. Finally, it is proved that all states are uniformly ultimately bounded (UUB) by Lyapunov and invariant set theory. The effectiveness of the proposed scheme is further demonstrated by the simulation results.

1. Introduction

In recent years, the development of unmanned aerial vehicle (UAV) technology has led to wide applications. However, single UAV provides limited capabilities, which may not be applicable to some highly complex tasks. Inspired by multiagent technology, researchers begin to investigate the application technology of multiple UAVs (multi-UAVs). Compared with a single UAV, multi-UAVs have more benefits in terms of forest fire monitoring, area detection, and disaster assistance. Unlike a single UAV, the cooperative control of multi-UAVs need the information from neighboring UAVs, which significantly increasing the control design challenge.

As the basis of multi-UAVs control, the cooperative control design is an important task. In the past few years, numerous research results of cooperative control have been reported. In [1], a cooperative control strategy for motion control of multiple unmanned vehicles was proposed, which can keep the formation during the motion. In [2], a novel distributed intermittent control framework for containment control of multiagent system was proposed, which can reduce the communication burden via a directed graph. In [3], the obstacle avoidance problem of multi-UAVs in multiple obstacle environment was studied. In [4], a robust adaptive control strategy for cooperative control of UAVs under the decentralized communication network was proposed against uncertainty. In [5], the authors investigated the cooperative transport control problem using multirotor UAVs. In [6], a system analysis method was proposed for the tracking control problem of multi-UAVs. The distributed framework was used to describe the dynamic model of UAV, and the information of nodes and networks were considered in the distributed control design. [7] studied the output feedback formation control of multi-UAVs without velocity and angular velocity sensors, which were obtained via the state observer. However, the above researches only focused on the distributed control of the first-order or second-order systems, and there exist few research on the cooperative control of fixed-wing UAVs with high-order nonlinear characteristics.

In addition, the number of components in the multi-UAV system is more than that of a single UAV. Therefore,

the probability of multi-UAVs suffering from the actuator, sensor, or component faults is higher than that of a single UAV. At present, many research results show that the incidence of actuator fault in flight is the highest. Therefore, many scholars mainly focus on actuator faults [8, 9]. The probability of actuator fault occurred in the multi-UAVs will also increase due to the fact that the number of actuators is significantly increased. When an actuator fault of a UAV in the communication network occurs and is not handled in time, it will reduce the stability and threaten the safety of all UAVs [10], making the investigation on fault-tolerant cooperative control (FTCC) a necessary task. In [11], based on the design of inner-outer-loop control and back-stepping control, an FTCC strategy was designed for multi-UAVs against permanent faults. In [12], Yu et al. further studied the FTCC design method of multi-UAVs by using a similar control framework of reference generator technology. It should be emphasized that the results [11, 12] are about the FTCC scheme of multi-UAVs under the master-slave framework, which cannot be directly applied to the distributed cooperative control design. Considering the diversity of research on cooperative control of multi-UAVs in the communication network, the FTCC scheme for multi-UAVs under distributed communication network needs to be further investigated.

Moreover, the actual multi-UAV system often encounters some problems such as input saturation, inaccurate aerodynamic parameters, and external interference, which lead to system instability or performance degradation [13–16]. Recently, many results have been reported to solve the problem of input saturation. In [17], a piecewise auxiliary system was introduced to deal with the asymmetric input constraints for a class of uncertain multi-input and multi-output nonlinear systems. Then, the auxiliary system was further used to deal with the force and moment constraints on ship [18]. In [19], another auxiliary signal was constructed using the error between the desired control input and the saturation control input. In [20], to solve the disadvantages of conventional methods based on the hyperbolic tangent function, an nth-order auxiliary dynamic system was skillfully constructed to avoid the effect of input saturation.

It should be emphasized that although numerous studies have been reported on the above literature, few results have studied the input saturation, inaccurate aerodynamic parameters, and external interference encountered by multi-UAVs in distributed communication networks at the same time. However, such factors are inevitable in the formation flight of multi-UAVs. If these factors are not solved in time, it may lead to the instability of the networked UAV system.

Furthermore, due to physical limitations, UAV states should be constrained. However, control strategies developed recently for multi-UAVs in the distributed communication network rarely consider these constraints on the states. Based on the above discussion, this paper proposes a distributed FTCC scheme for multi-UAVs under the distributed communication network with input saturation, state constraints, actuator faults, and unknown dynamics. In this work, to avoid the difficulty in designing the control policy due to the input saturation, an auxiliary control signal is designed to transform the restricted input. To handle the full-state constraint problem, virtual control signals are defined to replace the constraints, which can simplify the back-stepping design. For the unknown nonlinear dynamics caused by actuator faults and other unknown uncertainties, disturbance observer (DO) is designed for providing the estimation, while a recurrent wavelet fuzzy neural network (RWFNN) is adopted to further compensate the estimation error. In the RWFNN, the online adaptive learning strategy of parameters is designed based on the Lyapunov theory. Compared with other existing works, the main contributions of this paper are as follows:

(1) In [21–23], actuator faults, input saturation, output constraints, and external disturbances were considered, while the state constraints were not taken into account. To obtain satisfactory control performance against such factors, the FTCC scheme is designed in this paper by simultaneously considering the state constraints, actuator faults, and external disturbances.

(2) Compared with [24–27], which assessed uncertainty dynamics by designing a DO without compensation of the DO estimation error, this work further adopts an RWFNN to offset the estimation error, in which the parameters are updated by the proposed online learning strategy.

The organization of this paper is arranged as follows. Section 2 describes the preliminaries and problem statement. The design process of the FTCC scheme and the stability analysis are given in Section 3. Section 4 shows the simulation results and analysis. Finally, the conclusion is drawn in Section 5.

2. Preliminaries and Problem Statement

2.1. System Dynamics. In this paper, the cooperative control of N UAVs is investigated. The set of UAVs is denoted as $\Omega = \{1, 2, \cdots, N\}$, and the position dynamics of the ith UAV is described as

$$\begin{cases} \dot{x}_i = V_i \cos\gamma_i \cos\chi_i, \\ \dot{y}_i = V_i \cos\gamma_i \sin\chi_i, \\ \dot{z}_i = V_i \sin\gamma_i, \end{cases} \tag{1}$$

where $i \in \Omega$, x_i, y_i, and z_i are the positions. V_i, γ_i, and χ_i are velocity, flight path angle, and heading angle, respectively.

The aerodynamic force equations are given by

$$\begin{cases} \dot{V}_i = \dfrac{1}{m_i}(-D_i + T_i \cos\alpha_i \cos\beta_i) - g \sin\gamma_i, \\ \dot{\chi}_i = \dfrac{1}{m_i V_i \cos\gamma_i}((L_i \sin\mu_i + Y_i \cos\mu_i) + T_i(\sin\alpha_i \sin\mu_i - \cos\alpha_i \sin\beta_i \cos\mu_i)), \\ \dot{\gamma}_i = \dfrac{1}{m_i V_i}(L_i \cos\mu_i - Y_i \sin\mu_i) - \dfrac{g\cos\gamma_i}{V_i} + \dfrac{T_i}{m_i V_i}(\cos\alpha_i \sin\beta_i \sin\mu_i + \sin\alpha_i \cos\mu_i), \end{cases} \tag{2}$$

where $i \in \Omega$, m_i and g are the mass of the ith UAV and

gravitational coefficient, respectively; T_i, D_i, L_i, Y_i are the thrust, drag, lift, and lateral forces, respectively, and μ_i, α_i, and β_i are the bank angle, angle of attack, and sideslip angle, respectively.

The attitude kinematic model is expressed as

$$\begin{cases} \dot{\alpha}_i = q_i - \tan\beta_i(p_i\cos\alpha_i + r_i\sin\alpha_i), \\ \dot{\beta}_i = p_i\sin\alpha_i - r_i\cos\alpha_i + \dot{\chi}_i\cos\gamma_i\cdot\cos\mu_i - \dot{\gamma}_i\sin\mu_i, \\ \dot{\mu}_i = p_i\cos\alpha_i + \dfrac{r_i\sin\alpha_i}{\cos\beta_i} + \dot{\gamma}_i\cdot\cos\mu_i\tanh\beta_i + \dot{\chi}_i(\sin\gamma_i + \cos\gamma_i\sin\mu_i\tan\beta_i), \end{cases} \tag{3}$$

where $i \in \Omega$. p_i, q_i, and r_i are the angular rates.

The angular rate model is given as

$$\begin{cases} \dot{p}_i = (c_{i1}r_i + c_{i2}p_i)q_i + c_{i3}\mathscr{L}_i + c_{i4}\mathscr{N}_i, \\ \dot{q}_i = c_{i5}p_ir_i - c_{i6}\left(p_i^2 - r_i^2\right) + c_{i7}\mathscr{M}_i, \\ \dot{r}_i = (c_{i8}p_i - c_{i2}r_i)q_i + c_{i4}\mathscr{L}_i + c_{i9}\mathscr{N}_i, \end{cases} \tag{4}$$

where $i \in \Omega$. $\mathscr{L}_i$, $\mathscr{M}_i$, and $\mathscr{N}_i$ are roll, pitch, and yaw moments, respectively.

The forces T_i, D_i, L_i, and Y_i and the aerodynamic moments $\mathscr{L}_i$, $\mathscr{M}_i$, and $\mathscr{N}_i$ are expressed as

$$\begin{cases} T_i = T_{i\,\max}\delta_{T_i}, D_i = Q_is_iC_{iD}, \\ L_i = Q_is_iC_{iL}, Y_i = Q_is_iC_{iY}, \\ \mathscr{L}_i = Q_is_ib_iC_{i\mathscr{L}}, \mathscr{M}_i = Q_is_ic_iC_{i.\mathscr{M}}, \\ \mathscr{N}_i = Q_is_ib_iC_{i.\mathscr{N}}, \end{cases} \tag{5}$$

where $Q_i = \rho V_i^2/2$ is the dynamic pressure and s_i, b_i, and c_i represent the wing area, wing span, and mean aerodynamic chord, respectively. $T_{i\,\max}$ and δ_{T_i} are the maximum thrust and instantaneous thrust throttle setting, respectively. C_{iL}, C_{iD}, C_{iY}, $C_{i\mathscr{L}}$, $C_{i.\mathscr{M}}$, and $C_{i.\mathscr{N}}$ are given by

$$\begin{cases} C_{iL} = C_{iL0} + C_{iL\alpha}\alpha_i, \\ C_{iD} = C_{iD0} + C_{iD\alpha}\alpha_i + C_{iD\alpha^2}\alpha_i^2, \\ C_{iY} = C_{iY0} + C_{iY\beta}\beta_i, \end{cases} \tag{6}$$

$$\begin{cases} C_{i\mathscr{L}} = C_{i\mathscr{L}0} + C_{i\mathscr{L}\beta}\beta_i + C_{i\mathscr{L}\delta_a}\delta_{ia} + C_{i\mathscr{L}\delta_r}\delta_{ir} + \dfrac{C_{i\mathscr{L}p}b_ip_i + C_{i\mathscr{L}r}b_ir_i}{2V_i}, \\ C_{i.\mathscr{M}} = C_{i.\mathscr{M}0} + C_{i.\mathscr{M}\alpha}\alpha_i + C_{i.\mathscr{M}\delta_e}\delta_{ie} + \dfrac{C_{i.\mathscr{M}q}c_iq_i}{2V_i}, \\ C_{i.\mathscr{N}} = C_{i.\mathscr{N}0} + C_{i.\mathscr{N}\beta}\beta_i + C_{i.\mathscr{N}\delta_{ia}}\delta_{ia} + C_{i.\mathscr{N}\delta_r}\delta_{ir} + \dfrac{C_{i.\mathscr{N}p}b_ip_i}{2V_i} + \dfrac{C_{i.\mathscr{N}r}b_ir_i}{2V_i}, \end{cases} \tag{7}$$

where δ_{ia}, δ_{ie}, and δ_{ir} are aileron, elevator, and rudder deflections, respectively. C_{iL0}, $C_{iL\alpha}$, C_{iD0}, $C_{iD\alpha}$, $C_{iD\alpha^2}$, C_{iY0}, $C_{iY\beta}$, $C_{i\mathscr{L}0}$, $C_{i\mathscr{L}\beta}$, $C_{i\mathscr{L}\delta_a}$, $C_{i\mathscr{L}\delta_r}$, $C_{i\mathscr{L}p}$, $C_{i\mathscr{L}r}$, $C_{i.\mathscr{M}0}$, $C_{i.\mathscr{M}\alpha}$, $C_{i.\mathscr{M}\delta_e}$, $C_{i.\mathscr{M}q}$, $C_{i.\mathscr{N}0}$, $C_{i.\mathscr{N}\beta}$, $C_{i.\mathscr{N}\delta_a}$, $C_{i.\mathscr{N}\delta_r}$, $C_{i.\mathscr{N}p}$, and $C_{i.\mathscr{N}r}$ are aerodynamic derivatives. The definition of the inertial terms $c_{ij}(j = 1, 2, \cdots, 9)$ in (4) can be found in [28].

2.2. Control-Oriented Model. By defining $\mathbf{X}_{i1} = [\mu_i, \alpha_i, \beta_i]^T$, $\mathbf{X}_{i2} = [p_i, q_i, r_i]^T$, and $\mathbf{U}_i = [\delta_{1a}, \delta_{1e}, \delta_{1r}]^T$ and substituting (5), (6), and (7) into (1), (2), (3), and (4), then it follows that

$$\dot{\mathbf{X}}_{i1} = \mathbf{F}_{i1} + \mathbf{G}_{i1}\mathbf{X}_{i2} \tag{8}$$

$$\dot{\mathbf{X}}_{i2} = \mathbf{F}_{i2} + \mathbf{G}_{i2}\mathbf{U}_i \tag{9}$$

where $\mathbf{F}_{i1}$, $\mathbf{G}_{i1}$, $\mathbf{F}_{i2}$, and $\mathbf{G}_{i2}$ are given by

$$\mathbf{F}_{i1} = \begin{bmatrix} 0 & \sin\gamma_i + \cos\gamma_i\sin\mu_i\tan\beta_i & \cos\mu_i\tan\beta_i \\ 0 & -\dfrac{\cos\gamma_i\sin\mu_i}{\cos\beta_i} & -\dfrac{\cos\mu_i}{\cos\beta_i} \\ 0 & \cos\gamma_i\cos\mu_i & -\sin\mu_i \end{bmatrix} \begin{bmatrix} \dfrac{-D_i + T_i\cos\alpha_i\cos\beta_i}{m_i} - g\sin\gamma_i \\ \dfrac{1}{m_iV_i\cos\gamma_i}[L_i\sin\mu_i + Y_i\cos\mu_i + \\ T_i(\sin\alpha_i\sin\mu_i - \cos\alpha_i\sin\beta_i\cos\mu_i)] \\ -\dfrac{g\cos\gamma_i}{V_i} + \dfrac{1}{m_iV_i}[L_i\cos\mu_i - Y_i\sin\mu_i \\ +T_i(\cos\alpha_i\sin\beta_i\sin\mu_i + \sin\alpha_i\cos\mu_i)] \end{bmatrix},$$

$$\mathbf{G}_{i1} = \begin{bmatrix} \dfrac{\cos\alpha_i}{\cos\beta_i} & 0 & \dfrac{\sin\alpha_i}{\cos\beta_i} \\ -\cos\alpha_i\tan\beta_i & 1 & -\sin\alpha_i\tan\beta_i \\ \sin\alpha_i & 0 & -\cos\alpha_i \end{bmatrix},$$

$$\mathbf{F}_{i2} = [F_{i21}, F_{i22}, F_{i23}]^{\mathrm{T}}$$

$$\begin{cases} F_{i21} = c_{i1}q_ir_i + c_{i2}p_iq_i + c_{i3}\bar{q}_is_ib_i\left(C_{i\mathscr{L}0} + C_{i\mathscr{L}\beta_i} + \dfrac{C_{i\mathscr{L}p}b_ip_i}{2V_i} + \dfrac{C_{i\mathscr{L}r}b_ir_i}{2V_i}\right) \\ F_{i22} = c_{i5}p_ir_i - c_{i6}\left(p_i^2 - r_i^2\right) + c_{i7}\bar{q}_is_ic_i\left(C_{i.\mathscr{M}0} + C_{i.\mathscr{M}\alpha}\alpha_i + \dfrac{C_{i.\mathscr{M}q}c_iq_i}{2V_i}\right) \\ F_{i23} = c_{i8}p_iq_i - c_{i2}q_ir_i + c_{i4}\bar{q}_is_ib_i\left(C_{i\mathscr{L}0} + C_{i\mathscr{L}\beta}\cdot\beta_i + \dfrac{C_{i\mathscr{L}p}b_ip_i}{2V_i} + \dfrac{C_{i\mathscr{L}r}b_ir_i}{2V_i}\right) + c_{i9}\bar{q}_is_ib_i\cdot\left(C_{i.\mathscr{N}0} + C_{i.\mathscr{N}\beta_i} + \dfrac{C_{i.\mathscr{N}p}b_ip_i}{2V_i} + \dfrac{C_{i.\mathscr{N}r}b_ir_i}{2V_i}\right) \end{cases}$$

$$\begin{cases} \mathbf{G}_{i2} = \begin{bmatrix} a_{11} & 0 & a_{13} \\ 0 & a_{22} & 0 \\ a_{31} & 0 & a_{33} \end{bmatrix}, \\ a_{11} = c_{i3}\bar{q}_i s_i b_i C_{i\mathscr{L}\delta_a} + c_{i4}\bar{q}_i s_i b_i C_{i\mathscr{N}\delta_a}, \\ a_{13} = c_{i3}\bar{q}_i s_i b_i C_{i\mathscr{L}\delta_r} + c_{i4}\bar{q}_i s_i b_i C_{i\mathscr{N}\delta_r}, \\ a_{22} = c_{i7}\bar{q}_i s_i c_i C_{i\mathscr{M}\delta_e}, \\ a_{31} = c_{i4}\bar{q}_i s_i b_i C_{i\mathscr{L}\delta_a} + c_{i9}\bar{q}_i s_i b_i C_{i\mathscr{N}\delta_a}, \\ a_{33} = c_{i4}\bar{q}_i s_i b_i C_{i\mathscr{L}\delta_r} + c_{i9}\bar{q}_i s_i b_i C_{i\mathscr{N}\delta_r}. \end{cases} \tag{10}$$

It can be seen that $\mathbf{F}_{i2}$ and $\mathbf{G}_{i2}$ have many aerodynamic parameters. However, it is difficult to obtain accurate aerodynamic parameters of UAVs in practical engineering applications. To facilitate the design of the controller, $\mathbf{F}_{i2}$ and $\mathbf{G}_{i2}$ can be decomposed into known items $\mathbf{F}_{i20}$, $\mathbf{G}_{i20}$ and unknown items $\Delta\mathbf{F}_{i2}$, $\Delta\mathbf{G}_{i2}$, respectively.

Then, the attitude model can be described as

$$\dot{\mathbf{X}}_{i1} = \mathbf{F}_{i1} + \mathbf{G}_{i1}\mathbf{X}_{i2}, \tag{11}$$

$$\dot{\mathbf{X}}_{i2} = \mathbf{F}_{i20} + \Delta\mathbf{F}_{i2} + (\mathbf{G}_{i20} + \Delta\mathbf{G}_{i2})\mathbf{U}_i, \tag{12}$$

where $\Delta\mathbf{F}_{i2}$, and $\Delta\mathbf{G}_{i2}$ are unknown nonlinear functions caused by the uncertain parameters, while $\mathbf{F}_{i1}$, $\mathbf{G}_{i1}$, $\mathbf{F}_{i20}$, and $\mathbf{G}_{i20}$ are known functions.

Remark 1. Due to the physical constraints, the sideslip angle $\beta_i \neq \pm\pi/2$, and $\det(\boldsymbol{G}_{i1}) = -\sec\beta_i$, so $\boldsymbol{G}_{i1}$ is invertible. In addition, $\boldsymbol{G}_{i2}$ is related to aerodynamic parameters so that it is invertible in the flight envelope.

2.3. Actuator Fault and Input Saturation. In this paper, the actuator fault is considered, which includes gain and bias failures. Therefore, the fault model can be expressed as [29]

$$\mathbf{U}_i = \boldsymbol{\rho}_i\mathbf{U}_{i0} + \mathbf{U}_{\mathrm{if}}, \tag{13}$$

where $i \in \Omega$, $\mathbf{U}_{i0} = [u_{i01}, u_{i02}, u_{i03}]^T$ represents the designed control signal, and $\mathbf{U}_i = [\delta_{ia}, \delta_{ie}, \delta_{ir}]^T$ is the actual control signal. $\boldsymbol{\rho}_i = \mathrm{diag}\{\rho_{i1}, \rho_{i2}, \rho_{i3}\}$ with $0 < \rho_{i1}, \rho_{i2}, \rho_{i3} \leq 1$ represents the gain fault matrix, and $\mathbf{U}_{\mathrm{if}} \in \mathbb{R}^3$ represents bias fault vector.

In the practical application, the output of the actuator is limited. In order to avoid the incredible phenomenon caused by actuator saturation, the designed control signal $\mathbf{U}_{i0}$ needs to satisfy the following constraint:

$$u_{i0\tau\ \min} \leq u_{i0\tau} \leq u_{i0\tau\ \max}, \quad \tau = \{1, 2, 3\}, \tag{14}$$

where $\tau = \{1, 2, 3\}$, $u_{i0\tau\ \max}$ is a positive constant and $u_{i0\tau\ \min}$ is a negative constant, which is the maximum and minimum allowable values for the actuator, respectively.

To solve input saturation problem, an auxiliary signal $\mathbf{v}_i = [v_{i1}, v_{i2}, v_{i3}]^T$ is used to get control signal $\mathbf{U}_{i0}(\mathbf{v}_i)$, and $\mathbf{U}_{i0}(v_i) = [u_{i01}(v_{i1}), u_{i02}(v_{i2}), u_{i03}(v_{i3})]^{\mathrm{T}}$, which is expressed as

$$u_{i0\tau}(v_{i\tau}) = \begin{cases} u_{i0\tau\ \max}\tanh\left(\dfrac{v_{i\tau}}{u_{i0\tau\ \max}}\right), v_{i\tau} \geq 0, \\ u_{i0\tau\ \min}\tanh\left(\dfrac{v_{i\tau}}{u_{i0\tau\ \min}}\right), v_{i\tau} < 0. \end{cases} \tag{15}$$

By substituting (13) and (15) into (12), then the attitude model can be expressed as

$$\dot{\mathbf{X}}_{i1} = \mathbf{F}_{i1} + \mathbf{G}_{i1}\mathbf{X}_{i2}, \tag{16}$$

$$\dot{\mathbf{X}}_{i2} = \mathbf{F}_{i20} + \mathbf{G}_{i20}\mathbf{U}_{i0}(\mathbf{v}_i) + \mathbf{D}_i, \tag{17}$$

where $\mathbf{D}_i = \Delta\mathbf{F}_{i2} + \mathbf{G}_{i20}((\rho_i - \mathbf{I}_3)\mathbf{U}_{i0} + \mathbf{U}_{\mathrm{if}}) + \Delta\mathbf{G}_{i2}\mathbf{U}_i$ is an unknown nonlinear function. Due to $\mathbf{D}_i$ being related to auxiliary control signal $\mathbf{v}_i$, designing the observer of unknown function $\mathbf{D}_i$ for generating the control signal $\mathbf{v}_i$ will cause the problem of "algebraic ring," which is solved by introducing the following first-order filter:

$$\dot{\boldsymbol{v}}_i = -\boldsymbol{\Lambda}\boldsymbol{v}_i + \boldsymbol{\xi}, \tag{18}$$

where $\boldsymbol{\Lambda}$ is a diagnonal matrix with positive eigenvalue and $\boldsymbol{\xi}$ is an auxiliary control signal.

Remark 2. As shown in (13), the fault that occurs in the actuator will diminish its ability to provide control input. For example, the range of motion of the rudder surface can reach $-25 \sim 25$ deg in the normal state, while it may deteriorate into $-20 \sim 20$ deg after the fault occurs. It seems in the fault conditions the actuator is more likely to occur saturation, i.e., cannot reach to the expected control value. In this paper, the upper and lower boundaries of the control input are fixed to the values in the normal state of the actuator, and a hyperbolic function is used to prevent actuator saturation as shown in (15). Meanwhile, using virtual control signal $\mathbf{v}_i$ and $\boldsymbol{\xi}$ to generate the expected control signal $\mathbf{U}_{i0}$ and using RWFNN to evaluate uncertainty item $\mathbf{D}_i$ which contains the actuator bias section, even though the fault could occur, the system can still keep stable.

2.4. State Constraints. The states $\mathbf{X}_{i1} = [\mu_i, \alpha_i, \beta_i]^{\mathrm{T}}$ and $\mathbf{X}_{i2} = [p, q, r]^{\mathrm{T}}$ generally have constraints in the practical application. In this paper, such a problem has been concerned. Due to the fact that states $\mathbf{X}_{i1}$ and $\mathbf{X}_{i2}$ have limits, inspired by works [30, 31], a transformation is used to convert the restricted states $\mathbf{X}_{i1}$ and $\mathbf{X}_{i2}$ to unrestricted states $\mathbf{Z}_{i1}$ and $\mathbf{Z}_{i2}$:

$$Z_{i1\tau} = \ln\frac{X_{i1\tau} - \underline{X}_{i1\tau}}{\overline{X}_{i1\tau} - X_{i1\tau}}, \tag{19}$$

$$Z_{i2\tau} = \ln \frac{X_{i2\tau} - \underline{X}_{i2\tau}}{\bar{X}_{i2\tau} - X_{i2\tau}}, \tag{20}$$

where $\tau = 1, 2, 3$. $X_{i1\tau}$, $X_{i2\tau}$, $Z_{i1\tau}$ and $Z_{i2\tau}$ represent the τth element of $\mathbf{X}_{i1}$, $\mathbf{X}_{i2}$, $\mathbf{Z}_{i1}$, and $\mathbf{Z}_{i2}$, respectively. $\bar{X}_{i1\tau}$ and $\bar{X}_{i2\tau}$ represent maximum allowable range of the τth element of $\mathbf{X}_{i1}$ and $\mathbf{X}_{i2}$, respectively, while the $\underline{X}_{i1\tau}$ and $\underline{X}_{i2\tau}$ represent minimum allowable range of the τth element of $\mathbf{X}_{i1}$ and $\mathbf{X}_{i2}$, respectively.

Remark 3. Since (19) and (20) are bijective, $\mathbf{X}_{i1}$ and $\mathbf{X}_{i2}$ will always stay in their own limits if $\mathbf{Z}_{i1}$ and $\mathbf{Z}_{i2}$ are bounded on $\forall t \geq 0$.

2.5. Basic Graph Theory. In this paper, an undirected graph $\mathcal{G} = \{\mathcal{V}, \mathcal{C}, \mathcal{A}\}$ is used to describe the formation flight of N UAVs. The set of UAVs is described by $\mathcal{V} = \{v_1, v_2, \cdots, v_N\}$, $\mathcal{C} \subseteq \mathcal{V} \times \mathcal{V}$ represents the communication links between UAVs, and $\mathcal{A} \in R^{N\times N}$ is the adjacency matrix. If the link between the ith UAV and jth UAV exists, $a_{ij} = a_{ji} = 1$, which are the elements of $\mathcal{A}$. A path from the ith UAV to the kth UAV can be a sequence $v_i \longrightarrow v_j \longrightarrow v_k$, where $(v_i, v_j), (v_j, v_k) \in \mathcal{C}$. If there exists a path between any two UAVs, then $\mathcal{G}$ is a connected graph. A set is defined as $N_i = \{j : (v_i, v_j) \in \mathcal{C}, i \neq j\}$, and the degree matrix is defined as $\mathcal{D} = \text{diag}\{d_i\} \in \mathbb{R}^{N\times N}$, where $d_i = \sum_{j\in N_i} a_{ij}$. The Laplacian matrix $\mathcal{L} \in \mathbb{R}^{N\times N}$ is denoted as

$$\mathcal{L} = \mathcal{D} - \mathcal{A}. \tag{21}$$

Assumption 4. The undirected graph $\mathcal{G}$ containing N UAVs is connected.

Lemma 5. *Under Assumption 4, $\mathcal{L}$ and $\mathcal{L} + \text{diag}(\Omega)$ are symmetric and positive definite [32].*

2.6. Control Objective. In this paper, the control objective is to design an FTCC scheme for N UAVs, such that the attitude tracking error of each UAVs can be finally uniformly bounded, while the attitude $\mathbf{X}_{i1}$ and $\mathbf{X}_{i2}$ of all UAVs are always in limits, even when a portion of UAVs is subjected to actuator saturation and actuator faults.

3. Fault-Tolerant Cooperative Controller Design and Stability Analysis

In this section, the process of designing the FTCC scheme for N UAVs will be described. A main method adopted in the design is transforming the individual tracking error of each UAV to the synchronization tracking error.

3.1. Fault-Tolerant Cooperative Controller Design. Define the independent tracking error of ith UAV as $\tilde{\mathbf{Z}}_{i1} = \mathbf{Z}_{i1} - \mathbf{Z}_{i1d}$, then the cooperative tracking error of ith UAV is defined as

$$\mathbf{E}_{i1} = \lambda_1 \tilde{\mathbf{Z}}_{i1} + \lambda_2 \sum_{j\in N_i} a_{ij}\left(\tilde{\mathbf{Z}}_{i1} - \tilde{\mathbf{Z}}_{j1}\right), \tag{22}$$

where $\mathbf{E}_{i1} = [E_{i11}, E_{i12}, E_{i13}]^T$, λ_1 and λ_2 are positive parameters, which are used to regulate the cooperative tracking performance.

Using the Kronecker product "$\otimes$", and define $\mathbf{E}_1 = [\mathbf{E}_{11}^T, \mathbf{E}_{21}^T, \cdots, \mathbf{E}_{N1}^T]^T$, $\tilde{\mathbf{Z}}_1 = [\tilde{\mathbf{Z}}_{11}^T, \tilde{\mathbf{Z}}_{21}^T, \cdots, \tilde{\mathbf{Z}}_{N1}^T]^T$, then the cooperative tracking error of all UAVs can be expressed as

$$\mathbf{E}_1 = [(\lambda_1 \mathbf{I}_N + \lambda_2 \mathcal{L}) \otimes \mathbf{I}_3]\tilde{\mathbf{Z}}_1. \tag{23}$$

By recalling Lemma 5, it yields $\|\tilde{\mathbf{Z}}_1\| = \|[(\lambda_1 + \lambda_2\mathcal{L})^{-1} \otimes \mathbf{I}_3]\mathbf{E}_1\| \leq 1/(\sigma_{\min}(\lambda_1 + \lambda_2\mathcal{L}))\|\mathbf{E}_1\|$, where $\sigma_{\min}(\cdot)$ represents the minimum singular value of matrix "$\cdot$." Therefore, $\tilde{\mathbf{Z}}_1 \longrightarrow 0$ if $\mathbf{E}_1 \longrightarrow 0$.

Using (22), the synchronization error of each UAV $\mathbf{E}_{i1}$ can be expressed as

$$\mathbf{E}_{i1} = \left(\lambda_1 + \lambda_2 \sum_{j\in N_i}^{j\neq i} a_{ij}\right)\tilde{\mathbf{Z}}_{i1} - \lambda_2 \sum_{j\in N_i}^{j\neq i} a_{ij}\tilde{\mathbf{Z}}_{j1}. \tag{24}$$

Differentiating (24) yields

$$\begin{aligned}\dot{\mathbf{E}}_{i1} &= A_i\left(\mathbf{g}_{i1}(\mathbf{X}_{i1})\dot{\mathbf{X}}_{i1} - \mathbf{g}_{i1}(\mathbf{X}_{i1d})\dot{\mathbf{X}}_{i1d}\right) - \lambda_2 \sum_{j\in N_i}^{j\neq i} a_{ij}\dot{\tilde{\mathbf{Z}}}_{j1} \\ &= A_i\left(\mathbf{g}_{i1}(\mathbf{X}_{i1})\dot{\mathbf{X}}_{i1} - \mathbf{g}_{i1}(\mathbf{X}_{i1d})\dot{\mathbf{X}}_{i1d}\right) \\ &\quad - \lambda_2 \sum_{j\in N_i}^{j\neq i} a_{ij}\left(\mathbf{g}_{i1}\left(\mathbf{X}_{j1}\right)\dot{\mathbf{X}}_{j1} - \mathbf{g}_{i1}\left(\mathbf{X}_{j1d}\right)\dot{\mathbf{X}}_{j1d}\right),\end{aligned} \tag{25}$$

where $A_i = \lambda_1 + \lambda_2 \sum_{j\in N_i}^{j\neq i} a_{ij}$, $\mathbf{g}_{i1}(\mathbf{x})$ is $\mathbb{R}^3 \longrightarrow \mathbb{R}^{3\times 3}$, $\mathbf{x} = [x_1, x_2, x_3]^{\mathrm{T}}$, which is expressed as

$$\begin{cases} \mathbf{g}_{i1}(\mathbf{x}) = \text{diag}\{g_{i1\tau}(x_\tau)\}, \quad \tau = \{1, 2, 3\}, \\ g_{i1\tau}(x_\tau) = \dfrac{\bar{X}_{i1\tau} - \underline{X}_{i1\tau}}{(x_\tau - \underline{X}_{i1\tau})(\bar{X}_{i1\tau} - x_\tau)}. \end{cases} \tag{26}$$

Substituting (11) into (25) yields

$$\dot{\mathbf{E}}_{i1} = A_i\mathbf{g}_{i1}(\mathbf{X}_{i1})(\mathbf{F}_{i1} + \mathbf{G}_{i1}\mathbf{X}_{i2}) - A_i\mathbf{g}_{i1}(\mathbf{X}_{i1d})\dot{\mathbf{X}}_{i1d} - \lambda_2 \sum_{j\in N_i}^{j\neq i} a_{ij}\dot{\tilde{\mathbf{Z}}}_{j1}. \tag{27}$$

Based on the back-stepping control architecture, (27) can be expressed as

$$\begin{aligned}\dot{\mathbf{E}}_{i1} &= A_i\mathbf{g}_{i1}(\mathbf{X}_{i1})\mathbf{F}_{i1} - A_i\mathbf{g}_{i1}(\mathbf{X}_{i1d})\dot{\mathbf{X}}_{i1d} - \lambda_2 \sum_{j\in N_i}^{j\neq i} a_{ij}\dot{\tilde{\mathbf{Z}}}_{j1} \\ &\quad + A_i\mathbf{g}_{i1}(\mathbf{X}_{i1})\mathbf{G}_{i1} \cdot (\mathbf{X}_{i2} - \mathbf{Z}_{i2} + \mathbf{E}_{i2} + \mathbf{Z}_{i2d}),\end{aligned} \tag{28}$$

where $\mathbf{E}_{i2} = \mathbf{Z}_{i2} - \mathbf{Z}_{i2d}$ and $\mathbf{Z}_{i2d}$ is a virtual control signal.

By using a low-pass filter, one has

$$\dot{\mathbf{Z}}_{i2d} = -k_{\epsilon_1}\left(\mathbf{Z}_{i2d} - \bar{\mathbf{Z}}_{i2d}\right), \tag{29}$$

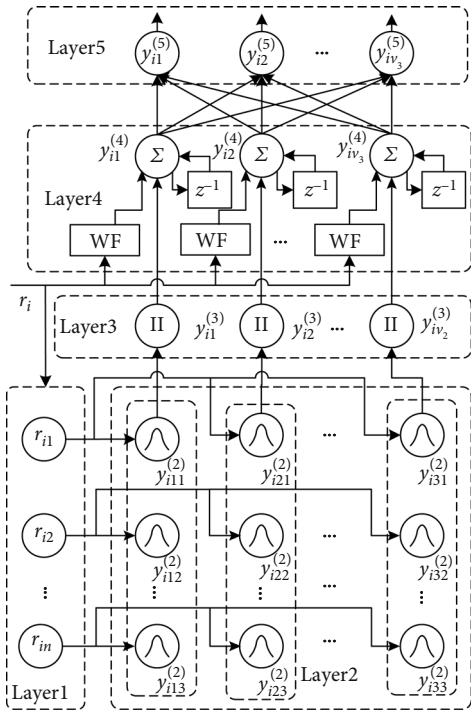

Figure 1: The structure of the RWFNN for each UAV.

where k_{ϵ_1} is a positive constant and $\bar{\mathbf{Z}}_{i2d}$ is an auxiliary signal, designed as

$$\bar{\mathbf{Z}}_{i2d} = (\mathbf{A}_i\mathbf{g}_{i1}(\mathbf{X}_{i1})\mathbf{G}_{i1})^{-1}\left(\lambda_2 \sum_{j\in N_i}^{j\neq i} a_{ij}\dot{\bar{\mathbf{Z}}}_{j1} - \mathbf{A}_i\mathbf{g}_{i1}(\mathbf{X}_{i1})(\mathbf{F}_{i1} + \mathbf{G}_{i1}(\mathbf{X}_{i2} - \mathbf{Z}_{i2})) + \mathbf{A}_i\mathbf{g}_{i1}(\mathbf{X}_{i1d})\dot{\mathbf{X}}_{i1d} - \mathbf{K}_{i1}\mathbf{E}_{i1}\right), \tag{30}$$

where $\mathbf{K}_{i1}$ is a positive diagonal matrix.

Defining the filtering error as $\boldsymbol{\epsilon}_{i1} = \mathbf{Z}_{i2d} - \bar{\mathbf{Z}}_{i2d}$, one can obtain

$$\dot{\boldsymbol{\epsilon}}_{i1} = -k_{\epsilon_{i1}}\boldsymbol{\epsilon}_{i1} - \dot{\bar{\mathbf{Z}}}_{i2d}. \tag{31}$$

By substituting (30) into (28), one can obtain

$$\begin{aligned}\mathbf{E}_{i1}^T\dot{\mathbf{E}}_{i1} \le{}& -\mathbf{E}_{i1}^{\mathrm{T}}\mathbf{K}_{i1}\mathbf{E}_{i1} + \mathbf{E}_{i1}^{\mathrm{T}}A_i\mathbf{g}_{i1}(\mathbf{X}_{i1})\mathbf{G}_{i1}\cdot\mathbf{E}_{i2} \\ &+ \frac{1}{2h_{i1}}\left\|\mathbf{E}_{i1}^{\mathrm{T}}A_i\mathbf{g}_{i1}(\mathbf{X}_{i1})\mathbf{G}_{i1}\right\|^2 + \frac{h_{i1}}{2}\|\boldsymbol{\epsilon}_{i1}\|^2,\end{aligned} \tag{32}$$

where h_{i1} is a positive constant and $\|\cdot\|$ represents 2-norm of vector.

To estimate the unknown function $\mathbf{D}_i$ of each UAV, the following DO is designed for the ith UAV:

$$\hat{\mathbf{D}}_i = k_2\left(\mathbf{X}_{i2} - \hat{\mathbf{X}}_{i2}\right) + k_1k_2\int\left(\mathbf{X}_{i2} - \hat{\mathbf{X}}_{i2}\right)\mathrm{d}t, \tag{33}$$

$$\dot{\hat{\mathbf{X}}}_{i2} = \mathbf{F}_{i20} + \mathbf{G}_{i20}\mathbf{U}_{i0}(\mathbf{v}_i) + \hat{\mathbf{D}}_i + k_1\left(\mathbf{X}_{i2} - \hat{\mathbf{X}}_{i2}\right), \tag{34}$$

where k_1 and k_2 are positive parameters, $\hat{\mathbf{D}}_i$ is the estimate of $\mathbf{D}_i$.

Define $\mathbf{e}_{X_{i2}} = \mathbf{X}_{i2} - \hat{\mathbf{X}}_{i2}$ and $\tilde{\mathbf{D}}_i = \mathbf{D}_i - \hat{\mathbf{D}}_i$, one can obtain

$$\dot{\mathbf{e}}_{X_{i2}} + k_1\mathbf{e}_{X_{i2}} = \tilde{\mathbf{D}}_i. \tag{35}$$

Taking the derivative of (35) and using (33) give

$$\dot{\tilde{\mathbf{D}}}_i + k_2\tilde{\mathbf{D}}_i = \dot{\mathbf{D}}. \tag{36}$$

From (36), it can be known that the estimation error $\tilde{\mathbf{D}}_i$ will not converge to zero since $\dot{\mathbf{D}} \neq 0$. In order to estimate the unknown function $\mathbf{D}_i$ more accurate, a five-layer RWFNN is used to estimate the error $\tilde{\mathbf{D}}_i$ of the DO with defining $\boldsymbol{\Delta}_i = \tilde{\mathbf{D}}_i$.

The RWFNN structure is illustrated in Figure 1, including five layers (input layer, membership layer, rule layer, composite layer, and output layer) [33]. The components of the RWFNN are introduced as follows:

Layer 1–Input Layer: Input layer is the first layer, where $\mathbf{r}_i = [r_{i1}, r_{i2}, \cdots, r_{iv_1}]^T$ is the input features of RWFNN. The output of layer 1 is expressed as

$$y_{ij}^{(1)} = r_{ij}, \tag{37}$$

where $j \in \{1, 2, \cdots, v_1\}$, v_1 is the dimension of input features, and $y_{ij}^{(1)}$ represents the output of jth neuron of Layer 1.

Layer 2–Membership Layer: Layer 2 has v_1 rows and v_2 columns, and its output can be described as

$$y_{ijk}^{(2)} = e^{-\left(y_{ij}^{(1)} - c_{ijk}\right)^2/\sigma_{ijk}^2}, \tag{38}$$

where $j \in \{1, 2, \cdots, v_1\}$, $k \in \{1, 2, \cdots, v_2\}$. v_2 is a positive constant, depending on the number of neurons. $y_{ijk}^{(2)}$ denotes the neuron of layer 2 in row j, column k.

Layer 3–Rule Layer: Layer 3 has v_2 neurons, and the output of layer 3 is described as

$$y_{ik}^{(3)} = \prod_{j=1}^{v_1} y_{ijk}^{(2)}, \tag{39}$$

where $k \in \{1, 2, \cdots, v_2\}$, and $y_{ik}^{(3)}$ denotes the kth neuron of Layer 3.

Layer 4–Composite Layer: Layer 4 also has v_2 neurons, and the input of Layer 4 consists the output of the wavelet layer, recurrent layer, and Layer 2, where the output of wavelet layer is described as

$$\begin{aligned}\psi_{ik} &= \sum_{j=1}^{v_1} w_{ijk}^F\phi_{ijk}(r_{ij}), \\ \phi_{ijk}(r_{ij}) &= \frac{1}{\sqrt{b_{ijk}}}\left[1 - \frac{\left(r_{ij} - a_{ijk}\right)^2}{b_{ijk}^2}\right]e^{-\left(r_{ij} - a_{ijk}\right)^2/2b_{ijk}^2},\end{aligned} \tag{40}$$

where $j \in \{1, 2, \cdots, v_1\}$, $k \in \{1, 2, \cdots, v_2\}$, ϕ_{ijk} is the output of

the jth neuron of Layer 1 to kth neuron of wavelet layer. ψ_{ik} represents the output of kth neuron of wavelet. w_{ijk}^F, a_{ijk}, and b_{ijk} represent the connecting weight, translation, and dilation variables, respectively.

The output of Layer 4 is expressed as

$$y_{ik}^{(4)} = y_{ik}^{(3)} \psi_{ik} w_{ik}^r y_{ik}^{(4)}(t-1), \tag{41}$$

where $y_{ik}^{(4)}$ is the output of kth neuron of Layer 4. w_{ik}^r and $y_{ik}^{(4)}(t-1)$ represent the recurrent weight and the output at the previous time step of the kth neuron, respectively.

Layer 5–Output Layer: Layer 5 has v_3 neurons, which determines the dimension of the final output. Each neuron's output of this layer is given by

$$y_{il}^{(5)} = \sum_{k=1}^{v_2} w_{ikl}^{(5)} y_{ik}^{(4)}, \tag{42}$$

where $l \in \{1, 2, \cdots, v_3\}$, $w_{ikl}^{(5)}$ is the connecting weight, and $y_{il}^{(5)}$ denotes the lth neuron of Layer 5.

Using (42), one can express $\mathbf{y}_i^{(5)}$ in the following vector form:

$$\mathbf{y}_i^{(5)} = \boldsymbol{\omega}_i^{(5)} \mathbf{y}_i^{(4)} \left(\boldsymbol{\omega}_i^r, \boldsymbol{\omega}_i^F, \mathbf{c}_i, \boldsymbol{\sigma}_i\right), \tag{43}$$

$y_{i1}^{(4)}, \cdots, dy_{ik}^{(4)}, \cdots, d_{iv_2}^{(4)}{}^{\mathrm{T}}] \in \mathbb{R}^{v_2 \times 1}$. $\boldsymbol{\omega}_i^{(5)} \in \mathbb{R}^{v_3 \times v_2}$, $\boldsymbol{\omega}_i^r \in \mathbb{R}^{v_2 \times 1}$, $\boldsymbol{\omega}_i^F \in \mathbb{R}^{v_1 v_2 \times 1}$, $\mathbf{c}_i \in \mathbb{R}^{v_1 v_2 \times 1}$, and $\boldsymbol{\sigma}_i \in \mathbb{R}^{v_1 v_2 \times 1}$, which are expressed as

$$\begin{aligned}
\boldsymbol{\omega}_i^{(5)} &= \left[\boldsymbol{\omega}_{i1}^5, \boldsymbol{\omega}_{i2}^{(5)}, \cdots, \boldsymbol{\omega}_{il}^{(5)}, \cdots, \boldsymbol{\omega}_{iv_3}^{(5)}\right]^T, \\
\boldsymbol{\omega}_{il}^{(5)} &= \left[\omega_{i1l}^{(5)}, \omega_{i2l}^{(5)}, \cdots, \omega_{ikl}^{(5)}, \cdots, \omega_{iv_2 l}^{(5)}\right]^T, \\
\boldsymbol{\omega}_i^r &= \left[\omega_{i1}^r, \omega_{i2}^r, \cdots, \omega_{ik}^r, \cdots, \omega_{iv_2}^r\right]^T, \\
\boldsymbol{\omega}_i^F &= \left[\boldsymbol{\omega}_{i1}^F, \boldsymbol{\omega}_{i2}^F, \cdots, \boldsymbol{\omega}_{ik}^F, \cdots, \boldsymbol{\omega}_{iv_2}^F\right]^T, \\
\boldsymbol{\omega}_{ik}^F &= \left[\omega_{i1k}^F, \omega_{i2k}^F, \cdots, \omega_{ijk}^F, \cdots, \omega_{iv_1 k}^F\right], \\
\mathbf{c}_i &= \left[\mathbf{c}_{i1}, \mathbf{c}_{i2}, \cdots, \mathbf{c}_{ik}, \cdots, \mathbf{c}_{iv_2}\right]^T, \\
\mathbf{c}_{ik} &= \left[c_{i1k}, c_{i2k}, \cdots, c_{ijk}, \cdots, c_{iv_1 k}\right], \\
\boldsymbol{\sigma}_i &= \left[\boldsymbol{\sigma}_{i1}, \boldsymbol{\sigma}_{i2}, \cdots, \boldsymbol{\sigma}_{ik}, \cdots, \boldsymbol{\sigma}_{iv_2}\right]^T, \\
\boldsymbol{\sigma}_{ik} &= \left[\sigma_{i1k}, \sigma_{i2k}, \cdots, \sigma_{ijk}, \cdots, \sigma_{iv_1 k}\right].
\end{aligned} \tag{44}$$

In this paper, v_3 is set as 3 due to the fact that the estimated variable $\boldsymbol{\Delta}_i$ is three-dimensional. Therefore, there exist optimal values $\boldsymbol{\omega}_i^{(5)*}$, $\boldsymbol{\omega}_i^{r*}$, $\boldsymbol{\omega}_i^{F*}$, $\mathbf{c}_i^*$, and $\boldsymbol{\sigma}_i^*$, such that

$$\boldsymbol{\Delta}_i = \mathbf{y}_i^{(5)*} + \varepsilon_{i1} = \boldsymbol{\omega}_i^{(5)*} \mathbf{y}_i^{(4)*} \left(\boldsymbol{\omega}_i^{r*}, \boldsymbol{\omega}_i^{F*}, \mathbf{c}_i^*, \boldsymbol{\sigma}_i^*\right) + \varepsilon_{i1}, \tag{45}$$

where ε_{i1} is the approximation error.

To design the adaptive law of weights for estimating the unknown item, it is needed to obtain the gradient of $\mathbf{y}_i^{(5)}$ of its variables firstly.

Differentiating both sides of $\mathbf{y}_i^{(5)}$, one can obtain

$$d\mathbf{y}_i^{(5)} = d\boldsymbol{\omega}_i^{(5)} \cdot \mathbf{y}_i^{(4)} + \boldsymbol{\omega}_i^{(5)} d\mathbf{y}_i^{(4)}, \tag{46}$$

To yield $d\mathbf{y}_i^{(4)}$, by the same way, differentiating both sides of $y_{ik}^{(4)}$, then

$$dy_{ik}^{(4)} = dy_{ik}^{(3)}(\mathbf{c}_{ik}, \boldsymbol{\sigma}_{ik}) + d\psi_{ik}\left(\boldsymbol{\omega}_{ik}^F\right) + d\left(\omega_{ik}^r y_{ik}^{(4)}(t-1)\right). \tag{47}$$

For term $dy_{ik}^{(3)}$, one can obtain it by combining (37), (38), and (39), that is

$$\begin{aligned}
dy_{ik}^{(3)} &= \sum_{j=1}^{v_1} \left(dc_{ijk} \cdot \frac{2\left(y_{ij}^{(1)} - c_{ijk}\right)}{\sigma_{ijk}^2} \prod_{j=1}^{v_1} y_{ijk}^{(2)} \right) \\
&\quad + \sum_{j=1}^{v_1} \left(d\sigma_{ijk} \cdot \frac{2\left(y_{ij}^{(1)} - c_{ijk}\right)^2}{\sigma_{ijk}^3} \prod_{j=1}^{v_1} y_{ijk}^{(2)} \right) \\
&= 2\left(\mathbf{y}_i^{(1)\mathrm{T}} - \mathbf{c}_{ik}\right) \diamond (\boldsymbol{\sigma}_{ik})^2 \cdot \prod_{j=1}^{v_1} y_{ijk}^{(2)} . d\mathbf{c}_{ik}^T \\
&\quad + 2\left(\mathbf{y}_i^{(1)\mathrm{T}} - \mathbf{c}_{ik}\right)^2 \diamond (\boldsymbol{\sigma}_{ik})^3 . \prod_{j=1}^{v_1} y_{ijk}^{(2)} \cdot d\boldsymbol{\sigma}_{ik}^T,
\end{aligned} \tag{48}$$

where "$\diamond$" represents dot division between matrices, and "$(*)^n$" represent the aligned "$*$" itself does n times dot product. And the $\mathbf{c}_{ik}$ and $\boldsymbol{\sigma}_{ik}$ have been defined in (44).

For the term $d\psi_{ik}$ and $d(\omega_{ik}^r y_{ik}^{(4)}(t-1))$, there exists

$$\begin{aligned}
d\boldsymbol{\psi}_{ik} &= d\left(\sum_{j=1}^{v_1} \omega_{ijk}^F \phi_{ijk}\left(r_{ij}\right)\right) \\
&= \sum_{j=1}^{v_1} \left(\phi_{ijk}\left(r_{ij}\right) \cdot d\omega_{ijk}^F\right) = \boldsymbol{\phi}_{ik} \cdot d\boldsymbol{\omega}_{ik}^{F\mathrm{T}},
\end{aligned} \tag{49a}$$

$$d\left(\omega_{ik}^r y_{ik}^{(4)}(t-1)\right) = y_{ik}^{(4)}\Big|_{t-1} \cdot d\omega_{ik}^r. \tag{49b}$$

Then, by combining (50), (48), and (49), $dy_{ik}^{(4)}$ can be expressed as

$$dy_{ik}^{(4)} = \boldsymbol{\Gamma}_{ik}^c d\mathbf{c}_{ik}^T + \boldsymbol{\Gamma}_{ik}^\sigma d\boldsymbol{\sigma}_{ik}^T + \boldsymbol{\Gamma}_{ik}^F d\boldsymbol{\omega}_{ik}^{F\mathrm{T}} + \Gamma_{ik}^r d\omega_{ik}^r, \tag{50}$$

where

$$\begin{cases} \boldsymbol{\Gamma}_{ik}^{c} = 2\left(\mathbf{y}_i^{(1)T} - \mathbf{c}_{ik}\right) \diamond (\boldsymbol{\sigma}_{ik})^2 \cdot \prod_{j=1}^{v_1} y_{ijk}^{(2)}, \\ \boldsymbol{\Gamma}_{ik}^{\sigma} = 2\left(\mathbf{y}_i^{(1)T} - \mathbf{c}_{ik}\right)^2 \diamond (\boldsymbol{\sigma}_{ik})^3 \cdot \prod_{j=1}^{v_1} y_{ijk}^{(2)}, \\ \boldsymbol{\Gamma}_{ik}^{F} = \phi_{ik}, \\ \Gamma_{ik}^{r} = y_{ik}^{(4)}\Big|_{t-1}. \end{cases} \tag{51}$$

Using (50) and (51), one can further write $d\mathbf{y}_i^{(4)}$ as

$$d\mathbf{y}_i^{(4)} = \boldsymbol{\Gamma}_i^{c} d\mathbf{c}_i + \boldsymbol{\Gamma}_i^{\sigma} d\boldsymbol{\sigma}_i + \boldsymbol{\Gamma}_i^{F} d\boldsymbol{\omega}_i^{F} + \boldsymbol{\Gamma}_i^{r} d\boldsymbol{\omega}_i^{r}, \tag{52}$$

where

$$\begin{aligned} \boldsymbol{\Gamma}_i^{c} &= \begin{bmatrix} \boldsymbol{\Gamma}_{i1}^{c} & \mathbf{0} & \cdots & \cdots & \cdots & \mathbf{0} \\ \mathbf{0} & \boldsymbol{\Gamma}_{i2}^{c} & \cdots & \cdots & \cdots & \mathbf{0} \\ \vdots & \vdots & \ddots & \vdots & \vdots & \vdots \\ \mathbf{0} & \cdots & \cdots & \boldsymbol{\Gamma}_{ik}^{c} & \cdots & \mathbf{0} \\ \vdots & \vdots & \vdots & \vdots & \ddots & \vdots \\ \mathbf{0} & \cdots & \cdots & \cdots & \cdots & \boldsymbol{\Gamma}_{iv_2}^{c} \end{bmatrix}, \\ \boldsymbol{\Gamma}_i^{\sigma} &= \begin{bmatrix} \boldsymbol{\Gamma}_{i1}^{\sigma} & \mathbf{0} & \cdots & \cdots & \cdots & \mathbf{0} \\ \mathbf{0} & \boldsymbol{\Gamma}_{i2}^{\sigma} & \cdots & \cdots & \cdots & \mathbf{0} \\ \vdots & \vdots & \ddots & \vdots & \vdots & \vdots \\ \mathbf{0} & \cdots & \cdots & \boldsymbol{\Gamma}_{ik}^{\sigma} & \cdots & \mathbf{0} \\ \vdots & \vdots & \vdots & \vdots & \ddots & \vdots \\ \mathbf{0} & \cdots & \cdots & \cdots & \cdots & \boldsymbol{\Gamma}_{iv_2}^{\sigma} \end{bmatrix}, \\ \boldsymbol{\Gamma}_i^{F} &= \begin{bmatrix} \boldsymbol{\Gamma}_{i1}^{F} & \mathbf{0} & \cdots & \cdots & \cdots & \mathbf{0} \\ \mathbf{0} & \boldsymbol{\Gamma}_{i2}^{F} & \cdots & \cdots & \cdots & \mathbf{0} \\ \vdots & \vdots & \ddots & \vdots & \vdots & \vdots \\ \mathbf{0} & \cdots & \cdots & \boldsymbol{\Gamma}_{ik}^{F} & \cdots & \mathbf{0} \\ \vdots & \vdots & \vdots & \vdots & \ddots & \vdots \\ \mathbf{0} & \cdots & \cdots & \cdots & \cdots & \boldsymbol{\Gamma}_{iv_2}^{F} \end{bmatrix}, \\ \boldsymbol{\Gamma}_i^{r} &= \begin{bmatrix} \Gamma_{i1}^{r} & 0 & \cdots & \cdots & \cdots & 0 \\ 0 & \Gamma_{i2}^{r} & \cdots & \cdots & \cdots & 0 \\ \vdots & \vdots & \ddots & \vdots & \vdots & \vdots \\ 0 & \cdots & \cdots & \Gamma_{ik}^{r} & \cdots & 0 \\ \vdots & \vdots & \vdots & \vdots & \ddots & \vdots \\ 0 & \cdots & \cdots & \cdots & \cdots & \Gamma_{iv_2}^{r} \end{bmatrix}. \end{aligned} \tag{53}$$

Moreover, using the property of Kronecker product, the term $d\boldsymbol{\omega}_i^{(5)} \cdot \mathbf{y}_i^{(4)}$ in (58) can be transformed to the following column vector form:

$$d\boldsymbol{\omega}_i^{(5)} \cdot \mathbf{y}_i^{(4)} = \left(\mathbf{I}_n \otimes \mathbf{y}_i^{(4)}\right) \cdot d\left(\mathrm{vec}\left(\boldsymbol{\omega}_i^{(5)T}\right)\right), \tag{54}$$

where "$\otimes$" represents Kronecker product, and "vec$(*)$" represents the operation that converts the aligned "$*$" to a column vector, that means

$$\mathrm{vec}\left(\boldsymbol{\omega}_i^{(5)\mathrm{T}}\right) = \left[\omega_{i1}^{(5)\mathrm{T}}, \cdots, \omega_{\mathrm{il}}^{(5)\mathrm{T}}, \cdots, \omega_{iv_3}^{(5)T}\right]^T. \tag{55}$$

To simplify the representation, using $\vec{\boldsymbol{\omega}}_i^{(5)}$ to represent $\mathrm{vec}(\boldsymbol{\omega}_i^{(5)T})$. Employing (58), (52), and (54) yeilds the following total differential equation:

$$\begin{aligned} d\mathbf{y}_i^{(5)} = \boldsymbol{\Gamma}_i^{5} d\vec{\boldsymbol{\omega}}_i^{(5)} + \boldsymbol{\omega}_i^{(5)} \boldsymbol{\Gamma}_i^{c} d\mathbf{c}_i + \boldsymbol{\omega}_i^{(5)} \boldsymbol{\Gamma}_i^{\sigma} d\boldsymbol{\sigma}_i \\ + \boldsymbol{\omega}_i^{(5)} \boldsymbol{\Gamma}_i^{F} d\boldsymbol{\omega}_i^{F} + \boldsymbol{\omega}_i^{(5)} \boldsymbol{\Gamma}_i^{r} d\boldsymbol{\omega}_i^{r}, \end{aligned} \tag{56}$$

where

$$\boldsymbol{\Gamma}_i^{5} = \mathbf{I}_n \otimes \mathbf{y}_i^{(4)}. \tag{57}$$

On the other hand, the total derivative of $d\mathbf{y}_i^{(5)}$ can be expressed as the following total differential form:

$$\begin{aligned} d\mathbf{y}_i^{(5)} = \left(\frac{\partial \mathbf{y}_i^{(5)}}{\partial \vec{\boldsymbol{\omega}}_i^{(5)}}\right)^T d\vec{\boldsymbol{\omega}}_i^{(5)} + \left(\frac{\partial \mathbf{y}_i^{(5)}}{\partial \mathbf{c}_i}\right)^{\mathrm{T}} d\mathbf{c}_i + \left(\frac{\partial \mathbf{y}_i^{(5)}}{\partial \boldsymbol{\sigma}_i}\right)^{\mathrm{T}} d\boldsymbol{\sigma}_i \\ + \left(\frac{\partial \mathbf{y}_i^{(5)}}{\partial \boldsymbol{\omega}_i^{F}}\right)^{\mathrm{T}} d\boldsymbol{\omega}_i^{F} + \left(\frac{\partial \mathbf{y}_i^{(5)}}{\partial \boldsymbol{\omega}_i^{r}}\right)^{\mathrm{T}} d\boldsymbol{\omega}_i^{r}. \end{aligned} \tag{58}$$

Hence, one can derive that

$$\begin{cases} \left(\dfrac{\partial \mathbf{y}_i^{(5)}}{\partial \vec{\boldsymbol{\omega}}_i^{(5)}}\right)^T = \boldsymbol{\Gamma}_i^{5}, \left(\dfrac{\partial \mathbf{y}_i^{(5)}}{\partial \mathbf{c}_i}\right)^T = \boldsymbol{\omega}_i^{(5)} \boldsymbol{\Gamma}_i^{c} \\ \left(\dfrac{\partial \mathbf{y}_i^{(5)}}{\partial \boldsymbol{\sigma}_i}\right)^T = \boldsymbol{\omega}_i^{(5)} \boldsymbol{\Gamma}_i^{\sigma}, \left(\dfrac{\partial \mathbf{y}_i^{(5)}}{\partial \boldsymbol{\omega}_i^{F}}\right)^T = \boldsymbol{\omega}_i^{(5)} \boldsymbol{\Gamma}_i^{F}, \\ \left(\dfrac{\partial \mathbf{y}_i^{(5)}}{\partial \boldsymbol{\omega}_i^{r}}\right)^T = \boldsymbol{\omega}_i^{(5)} \boldsymbol{\Gamma}_i^{r}. \end{cases} \tag{59}$$

Taking into account (58) and (59) and using the Taylor expansion, $\mathbf{y}_i^{(5)}$ can be expressed as

$$\begin{aligned} \mathbf{y}_i^{(5)} = \mathbf{y}_i^{(5)*} + \boldsymbol{\Gamma}_i^{5}\left(\vec{\boldsymbol{\omega}}_i^{(5)} - \vec{\boldsymbol{\omega}}_i^{(5)*}\right) + \boldsymbol{\omega}_i^{(5)} \boldsymbol{\Gamma}_i^{c}(\mathbf{c}_i - \mathbf{c}_i^{*}) + \boldsymbol{\omega}_i^{(5)} \boldsymbol{\Gamma}_i^{\sigma}(\boldsymbol{\sigma}_i - \boldsymbol{\sigma}_i^{*}) \\ + \boldsymbol{\omega}_i^{(5)} \boldsymbol{\Gamma}_i^{F}\left(\boldsymbol{\omega}_i^{F} - \boldsymbol{\omega}_i^{F*}\right) + \boldsymbol{\omega}_i^{(5)} \boldsymbol{\Gamma}_i^{r}(\boldsymbol{\omega}_i^{r} - \boldsymbol{\omega}_i^{r*}) + \varepsilon_{i2}. \end{aligned} \tag{60}$$

Using $\widehat{\boldsymbol{\Delta}}_i$ to estimate the unknown item $\boldsymbol{\Delta}_i$, and it is expressed as

$$\widehat{\boldsymbol{\Delta}}_i = \mathbf{y}_i^{(5)} + \operatorname{diag}\left(\operatorname{sign}\left(\mathbf{E}_{i2}^T \mathbf{g}_{i2}(\mathbf{X}_{i2})\right)\right)\widehat{\mathbf{H}}_i \triangleq \mathbf{y}_i^{(5)} + \boldsymbol{\Gamma}_i^H \widehat{\mathbf{H}}_i, \quad (61)$$

where $\boldsymbol{\Gamma}_i^H = \operatorname{diag}(\operatorname{sign}(\mathbf{E}_{i2}^{\mathrm{T}} \mathbf{g}_{i2}(\mathbf{X}_{i2})))$ and $\widehat{\mathbf{H}}_i$ is an estimated value and will be introduced later.

Defining $\tilde{\boldsymbol{\Delta}}_i = \widehat{\boldsymbol{\Delta}}_i - \boldsymbol{\Delta}_i$, $\tilde{\vec{\boldsymbol{\omega}}}_i^{(5)} = \vec{\boldsymbol{\omega}}_i^{(5)} - \vec{\boldsymbol{\omega}}_i^{(5)*}$, $\tilde{\mathbf{c}}_i = \mathbf{c}_i - \mathbf{c}_i^*$, $\tilde{\boldsymbol{\sigma}}_i = \boldsymbol{\sigma}_i - \boldsymbol{\sigma}_i^*$, $\tilde{\boldsymbol{\omega}}_i^F = \boldsymbol{\omega}_i^F - \boldsymbol{\omega}_i^{F*}$, and $\tilde{\boldsymbol{\omega}}_i^r = \boldsymbol{\omega}_i^r - \boldsymbol{\omega}_i^{r*}$ and combining (45), (60), and (61), it yeilds

$$\begin{aligned}\tilde{\boldsymbol{\Delta}}_i = {} & \boldsymbol{\Gamma}_i^5 \tilde{\vec{\boldsymbol{\omega}}}_i^{(5)} + \boldsymbol{\omega}_i^{(5)} \boldsymbol{\Gamma}_i^c \tilde{\mathbf{c}}_i + \boldsymbol{\omega}_i^{(5)} \boldsymbol{\Gamma}_i^\sigma \tilde{\boldsymbol{\sigma}}_i + \boldsymbol{\omega}_i^{(5)} \boldsymbol{\Gamma}_i^F \tilde{\boldsymbol{\omega}}_i^F \\ & + \boldsymbol{\omega}_i^{(5)} \boldsymbol{\Gamma}_i^r \tilde{\boldsymbol{\omega}}_i^r + \boldsymbol{\varepsilon}_{i2} - \boldsymbol{\varepsilon}_{i1} + \boldsymbol{\Gamma}_i^H \widehat{\mathbf{H}}_i.\end{aligned} \quad (62)$$

Taking the derivative of $\mathbf{E}_{i2}$ and using (17) and (20), one can obtain

$$\dot{\mathbf{E}}_{i2} = \dot{\mathbf{Z}}_{i2} - \dot{\mathbf{Z}}_{i2d} = \mathbf{g}_{i2}(\mathbf{X}_{i2})(\mathbf{F}_{i20} + \mathbf{G}_{i20}\mathbf{U}_{i0}(\mathbf{v}_i) + \mathbf{D}_i) - \dot{\mathbf{Z}}_{i2d}, \quad (63)$$

where $\mathbf{g}_{i2}(\mathbf{x})$ and $\mathbf{x} = [x_1, x_2, x_3]^{\mathrm{T}}$ are

$$\begin{cases} \boldsymbol{g}_{i2}(\boldsymbol{x}) = \operatorname{diag}\{g_{i2\tau}(x_\tau)\}, \tau = \{1, 2, 3\}, \\ g_{i2\tau}(x_\tau) = \dfrac{\bar{X}_{i2\tau} - \underline{X}_{i2\tau}}{(x_\tau - \underline{X}_{i2\tau})(\bar{X}_{i2\tau} - x_\tau)}. \end{cases} \quad (64)$$

By using the back-stepping method and defining $\mathbf{v}_{id}$ as a virtual control signal, then $\dot{\mathbf{E}}_{i2}$ can be expressed as

$$\begin{aligned}\dot{\mathbf{E}}_{i2} = {} & \mathbf{g}_{i2}(\mathbf{X}_{i2})(\mathbf{F}_{i20} + \mathbf{G}_{i20}\mathbf{v}_{id} + \mathbf{G}_{i20}(\mathbf{U}_{i0} - \mathbf{v}_i) \\ & + \mathbf{G}_{i20}\mathbf{E}_{i3} + \mathbf{D}_i) - \dot{\mathbf{Z}}_{i2d},\end{aligned} \quad (65)$$

where $\mathbf{E}_{i3} = \mathbf{v}_i - \mathbf{v}_{id}$. In order to reduce computational burden of taking time derivative for virtual control signal $\mathbf{v}_{id}$, a filter is used to obtain $\mathbf{v}_{id}$, which is given by

$$\dot{\mathbf{v}}_{id} = -k_{\epsilon_2}(\mathbf{v}_{id} - \bar{\mathbf{v}}_{id}), \quad (66)$$

where k_{ϵ_2} is a positive constant, and $\bar{\mathbf{v}}_{id}$ is an auxiliary signal, designed as

$$\begin{aligned}\bar{\mathbf{v}}_{id} = {} & (\mathbf{g}_{i2}(\mathbf{X}_{i2})\mathbf{G}_{i20})^{-1}\Big[-\mathbf{g}_{i2}(\mathbf{X}_{i2})\Big(\mathbf{F}_{i20} + \mathbf{G}_{i20}(\mathbf{U}_{i0}(\mathbf{v}_i) - \mathbf{v}_i) + \widehat{\mathbf{D}}_i + \widehat{\boldsymbol{\Delta}}_i + \widehat{\mathbf{H}}_i\Big) \\ & + \dot{\mathbf{Z}}_{i2d} - \mathbf{K}_{i2}\mathbf{E}_{i2} - A_i\mathbf{g}_{i1}(\mathbf{X}_{i1}) \cdot \mathbf{G}_{i1}\mathbf{E}_{i1}\Big],\end{aligned} \quad (67)$$

where $\mathbf{K}_{i2}$ is a positive diagonal matrix.

Define the filter error as $\boldsymbol{\epsilon}_{i2} = \mathbf{v}_{id} - \bar{\mathbf{v}}_{id}$, then one can obtain from (66) that

$$\dot{\boldsymbol{\epsilon}}_{i2} = -k_{\boldsymbol{\epsilon}_{i2}}\boldsymbol{\epsilon}_{i2} - \dot{\bar{\mathbf{v}}}_{id}. \quad (68)$$

Substituting (65) with (67) and (62), with considering $|\boldsymbol{\varepsilon}_{i1} - \boldsymbol{\varepsilon}_{i2}| \le \mathbf{H}_i$ in which $|*|$ represents the absolute value of the matrix "$*$", while defining $\widehat{\mathbf{H}}_i$ as the estimation of $\mathbf{H}_i$ and $\tilde{\mathbf{H}}_i = \mathbf{H} - \widehat{\mathbf{H}}_i$ as the estimation error, one can obtain

$$\begin{aligned}\boldsymbol{E}_{i2}^{\mathrm{T}}\dot{\boldsymbol{E}}_{i2} \le {} & -\boldsymbol{E}_{i2}^{\mathrm{T}}\boldsymbol{K}_{i2}\boldsymbol{E}_{i2} - \boldsymbol{E}_{i2}^{\mathrm{T}}\boldsymbol{A}_i\boldsymbol{g}_{i1}(\boldsymbol{X}_{i1})\boldsymbol{G}_{i1}\boldsymbol{E}_{i1} + \boldsymbol{E}_{i2}^{\mathrm{T}}\boldsymbol{g}_{i2}(\boldsymbol{X}_{i2}) \\ & \cdot \Big[\boldsymbol{G}_{i20}\boldsymbol{E}_{i3} + \boldsymbol{G}_{i20}\boldsymbol{\epsilon}_{i2} - \boldsymbol{\Gamma}_i^5 \cdot \dot{\tilde{\vec{\boldsymbol{\omega}}}}_i^{(5)} - \boldsymbol{\omega}_i^{(5)}\boldsymbol{\Gamma}_i^c\tilde{\mathbf{c}}_i - \boldsymbol{\omega}_i^{(5)}\boldsymbol{\Gamma}_i^\sigma\tilde{\boldsymbol{\sigma}}_i - \boldsymbol{\omega}_i^{(5)}\boldsymbol{\Gamma}_i^F\tilde{\boldsymbol{\omega}}_i^F - \boldsymbol{\omega}_i^{(5)}\boldsymbol{\Gamma}_i^r\tilde{\boldsymbol{\omega}}_i^r\Big] \\ & + \left|\boldsymbol{E}_{i2}^{\mathrm{T}}\boldsymbol{g}_{i2}(\boldsymbol{X}_{i2})\right|\tilde{\boldsymbol{H}}_i.\end{aligned} \quad (69)$$

Taking the time derivative of $\mathbf{E}_{i3}$ and using (18), one can obtain

$$\dot{\mathbf{E}}_{i3} = -\boldsymbol{\Lambda}\mathbf{v}_i + \boldsymbol{\xi} - \dot{\mathbf{v}}_{id}. \quad (70)$$

Design the auxiliary control signal $\boldsymbol{\xi}$ as

$$\boldsymbol{\xi} = \begin{cases} \boldsymbol{\Lambda}\boldsymbol{v}_i + \dot{\boldsymbol{v}}_{id} - \boldsymbol{K}_{i3}\boldsymbol{E}_{i3} - \boldsymbol{g}_{i2}(\boldsymbol{X}_{i2})\boldsymbol{G}_{i20}\boldsymbol{E}_{i2} - \dfrac{1}{\|\boldsymbol{E}_{i3}\|^2}\left(\dfrac{h_{i1}}{2}\|\boldsymbol{\epsilon}_{i1}\|^2 + \dfrac{h_{i2}}{2}\|\boldsymbol{\epsilon}_{i2}\|^2\right)\boldsymbol{E}_{i3}, \\ (\|\boldsymbol{E}_{i3}\|^2 > \mu_{ib}), \\ \boldsymbol{\Lambda}\boldsymbol{v}_i + \dot{\boldsymbol{v}}_{id} - \boldsymbol{K}_{i3}\boldsymbol{E}_{i3} - \boldsymbol{g}_{i2}(\boldsymbol{X}_{i2})\boldsymbol{G}_{i20}\boldsymbol{E}_{i2} - \dfrac{1}{\mu_{ib}}\left(\dfrac{h_{i1}}{2}\|\boldsymbol{\epsilon}_{i1}\|^2 + \dfrac{h_{i2}}{2}\|\boldsymbol{\epsilon}_{i2}\|^2\right)\boldsymbol{E}_{i3}, \\ (\|\boldsymbol{E}_{i3}\|^2 \le \mu_{ib}), \end{cases} \quad (71)$$

where $\mathbf{K}_{i3}$ is a positive diagonal matrix, and h_{i1} and h_{i2} are positive constants.

By combining (70) and (71), one has

$$\mathbf{E}_{i3}^T\dot{\mathbf{E}}_{i3} \le -\mathbf{E}_{i3}^T\mathbf{K}_{i3}\mathbf{E}_{i3} - \mathbf{E}_{i3}^T\mathbf{g}_{i2}(\mathbf{X}_{i2})\mathbf{G}_{i20}\mathbf{E}_{i2}. \quad (72)$$

Finally, the adaptive laws of RWFNN for the ith UAV are developed as

$$\begin{cases} \dot{\vec{\boldsymbol{\omega}}}_i^{(5)} = \eta_{i1}^{-1}\left[-\gamma_{i1}\vec{\boldsymbol{\omega}}_i^{(5)} + \left(\boldsymbol{E}_{i2}^{\mathrm{T}}\boldsymbol{g}_{i2}(\boldsymbol{X}_{i2})\boldsymbol{\Gamma}_i^5\right)^T\right], \\ \dot{\mathbf{c}}_i = \eta_{i2}^{-1}\left[-\gamma_{i2}\mathbf{c}_i + \left(\boldsymbol{E}_{i2}^{\mathrm{T}}\mathbf{g}_{i2}(\boldsymbol{X}_{i2})\boldsymbol{\omega}_i^{(5)}\boldsymbol{\Gamma}_i^c\right)^T\right], \\ \dot{\boldsymbol{\sigma}}_i = \eta_{i3}^{-1}\left[-\gamma_{i3}\boldsymbol{\sigma}_i + \left(\boldsymbol{E}_{i2}^{\mathrm{T}}\boldsymbol{g}_{i2}(\boldsymbol{X}_{i2})\boldsymbol{\omega}_i^{(5)}\boldsymbol{\Gamma}_i^\sigma\right)^T\right], \\ \dot{\boldsymbol{\omega}}_i^F = \eta_{i4}^{-1}\left[-\gamma_{i4}\boldsymbol{\omega}_i^F + \left(\boldsymbol{E}_{i2}^{\mathrm{T}}\boldsymbol{g}_{i2}(\boldsymbol{X}_{i2})\boldsymbol{\omega}_i^{(5)}\boldsymbol{\Gamma}_i^F\right)^T\right], \\ \dot{\boldsymbol{\omega}}_i^r = \eta_{i5}^{-1}\left[-\gamma_{i5}\boldsymbol{\omega}_i^r + \left(\boldsymbol{E}_{i2}^{\mathrm{T}}\boldsymbol{g}_{i2}(\boldsymbol{X}_{i2})\boldsymbol{\omega}_i^{(5)}\boldsymbol{\Gamma}_i^r\right)^T\right], \\ \dot{\widehat{\boldsymbol{H}}}_i = \eta_{i6}^{-1}\left[-\gamma_{i6}\widehat{\boldsymbol{H}}_i + \left|\boldsymbol{E}_{i2}^{\mathrm{T}}\boldsymbol{g}_{i2}(\boldsymbol{X}_{i2})\right|^T\right], \end{cases} \quad (73)$$

where $\gamma_{i1} \sim \gamma_{i5}$ are discontinuous switching constants to prevent the weights to infinity and γ_{i6} is a positive constant,

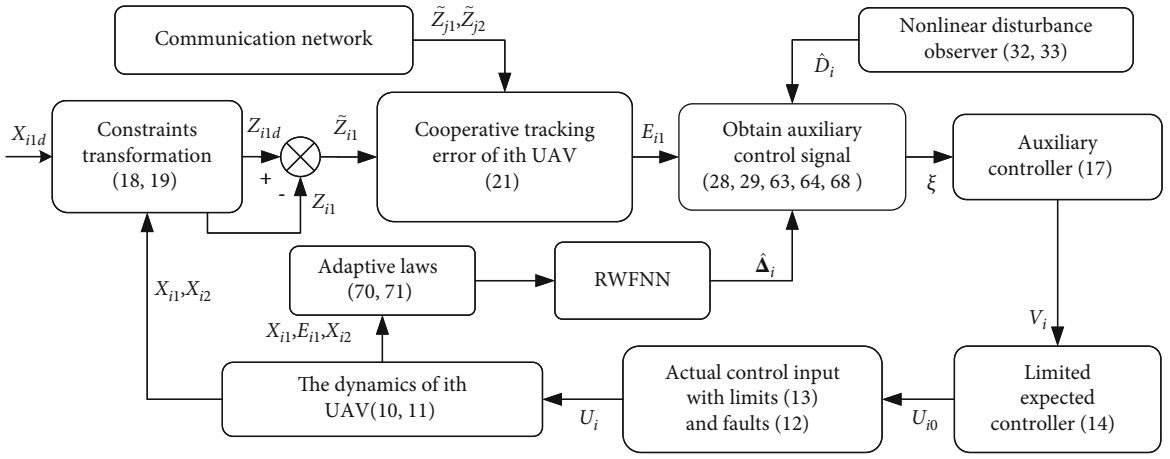

Figure 2: The proposed control scheme for the ith UAV.

where the switching constants are designed as

$$\gamma_{i1} = \begin{cases} 0 & \text{if } \left\|\vec{\boldsymbol{\omega}}_i^{(5)}\right\|^2 \le \bar{\omega}^{(5)}, \\ \bar{\gamma}_{i1} & \text{if } \left\|\vec{\boldsymbol{\omega}}_i^{(5)}\right\|^2 > \bar{\omega}^{(5)}, \end{cases} \tag{74a}$$

$$\gamma_{i2} = \begin{cases} 0 & \text{if } \|\boldsymbol{c}_i\|^2 \le \bar{c}, \\ \bar{\gamma}_{i2} & \text{if } \|\boldsymbol{c}_i\|^2 > \bar{c}, \end{cases} \tag{74b}$$

$$\gamma_{i3} = \begin{cases} 0 & \text{if } \|\boldsymbol{\sigma}_i\|^2 \le \bar{\sigma}, \\ \bar{\gamma}_{i3} & \text{if } \|\boldsymbol{\sigma}_i\|^2 > \bar{\sigma}, \end{cases} \tag{74c}$$

$$\gamma_{i4} = \begin{cases} 0 & \text{if } \left\|\boldsymbol{\omega}_i^F\right\|^2 \le \bar{\omega}_i^F, \\ \bar{\gamma}_{i4} & \text{if } \left\|\boldsymbol{\omega}_i^F\right\|^2 > \bar{\omega}_i^F, \end{cases} \tag{74d}$$

$$\gamma_{i5} = \begin{cases} 0 & \text{if } \|\boldsymbol{\omega}_i^r\|^2 \le \bar{\omega}_i^r, \\ \bar{\gamma}_{i5} & \text{if } \|\boldsymbol{\omega}_i^r\|^2 > \bar{\omega}_i^r, \end{cases} \tag{74e}$$

where $\bar{\omega}^{(5)}$, $\bar{c}$, $\bar{\sigma}$, $\bar{\omega}_i^F$, and $\bar{\omega}_i^r$ are positive constants, which represent the boundness of weight $\vec{\boldsymbol{\omega}}_i^{(5)}, \mathbf{c}_i, \boldsymbol{\sigma}_i, \boldsymbol{\omega}_i^F, \boldsymbol{\omega}_i^r$, respectively.

To this end, the proposed FTCC scheme is shown in Figure 2 to better illustrate the design principle and functional components in the control system.

Remark 6. Many papers choose multiplication on input and recurrence data as an operation on the neuron of the composite layer in RWFNN. However, it is sometimes problematic. For example, when inputs from layer 3 are minuscule, the outputs of the composite neuron will also become exceedingly small under multiplication. Under the limitation of computational precision, the outputs are equal to zero. Since the outputs will loop to the next multiplication, the outputs will always be zero, which causes neuron inactivation. Therefore, this paper uses the addition operation as an alternative, and the back-propagation gradient is deduced in detail using vectorized expressions, i.e., (46)–(59).

3.2. Stability Analysis

Theorem 7. *Consider the N UAVs (1)–(4) under the distributed communication network against the actuator faults (13), states constraints, and input saturation (15), if the control laws are chosen as (30), (67), and (71), the disturbance observers are developed as (33), and (34), and the adaptive laws are constructed as (73), (74a); then, all the states in the system are ultimately uniformly bounded and strictly confined within the limits.*

Proof. Choose a Lyapunov function as

$$\begin{aligned} V = \frac{1}{2}\sum_{i=1}^{N}\Big[& \boldsymbol{E}_{i1}^{\mathrm{T}}\boldsymbol{E}_{i1}^{\mathrm{T}} + \boldsymbol{E}_{i2}^{\mathrm{T}}\boldsymbol{E}_{i2}^{\mathrm{T}} + \boldsymbol{E}_{i3}^{\mathrm{T}}\boldsymbol{E}_{i3}^{\mathrm{T}} + \eta_{i1}\cdot\tilde{\vec{\boldsymbol{\omega}}}_i^{(5)\mathrm{T}}\tilde{\vec{\boldsymbol{\omega}}}_i^{(5)} \\ & + \eta_{i2}\tilde{\mathbf{c}}_i^{\mathrm{T}}\tilde{\mathbf{c}}_i + \eta_{i3}\tilde{\boldsymbol{\sigma}}_i^{\mathrm{T}}\boldsymbol{\sigma}_i + \eta_{i4}\cdot\tilde{\boldsymbol{\omega}}_i^{F\mathrm{T}}\tilde{\boldsymbol{\omega}}_i^F + \eta_{i5}\tilde{\boldsymbol{\omega}}_i^{r\mathrm{T}}\tilde{\boldsymbol{\omega}}_i^r \\ & + \eta_{i6}\tilde{\boldsymbol{H}}_i^{\mathrm{T}}\tilde{\boldsymbol{H}}_i + \boldsymbol{\epsilon}_{i1}^{\mathrm{T}}\cdot\boldsymbol{\epsilon}_{i1} + \boldsymbol{\epsilon}_{i2}^{\mathrm{T}}\boldsymbol{\epsilon}_{i2}\Big]. \end{aligned} \tag{75}$$

By taking the time derivative of V, combining (32), (69), (72), (31), and (68) and using Young inequality, one has

$$\begin{aligned} \dot{V} \le & \sum_{i=1}^{N}\left(-\mathbf{E}_{i1}^{\mathrm{T}}\mathbf{K}_{i1}\mathbf{E}_{i1} - \mathbf{E}_{i2}^{\mathrm{T}}\mathbf{K}_{i2}\mathbf{E}_{i2} - \mathbf{E}_{i3}^{\mathrm{T}}\mathbf{K}_{i3}\cdot\mathbf{E}_{i3}\right) \\ & + \sum_{i=1}^{N}\Bigg[\frac{1}{2h_{i1}}\left\|\mathbf{E}_{i1}^{\mathrm{T}}\mathbf{A}_i\mathbf{g}_{i1}(\mathbf{X}_{i1})\mathbf{G}_{i1}\right\|^2 + \frac{h_{i1}}{2}\|\boldsymbol{\epsilon}_{i1}\|^2 \\ & + \frac{1}{2h_{i2}}\left\|\mathbf{E}_{i1}^{\mathrm{T}}\mathbf{g}_{i2}(\mathbf{X}_{i2})\mathbf{G}_{i20}\right\|^2 + \frac{h_{i2}}{2}\|\boldsymbol{\epsilon}_{i2}\|^2 \\ & - \gamma_{i1}\tilde{\vec{\boldsymbol{\omega}}}_i^{(5)\mathrm{T}}\vec{\boldsymbol{\omega}}_i - \gamma_{i2}\tilde{\mathbf{c}}_i^{\mathrm{T}}\mathbf{c}_i - \gamma_{i3}\cdot\tilde{\boldsymbol{\sigma}}_i^{\mathrm{T}}\boldsymbol{\sigma}_i - \gamma_{i4}\tilde{\boldsymbol{\omega}}_i^{F\mathrm{T}}\boldsymbol{\omega}_i^F \\ & - \gamma_{i5}\tilde{\boldsymbol{\omega}}_i^{r\mathrm{T}}\boldsymbol{\omega}_i^r - \gamma_{i6}\tilde{\mathbf{H}}_i^{\mathrm{T}}\widehat{\mathbf{H}}_i - \left(k_{\epsilon_{i1}} - \frac{1}{2}\right)\|\boldsymbol{\epsilon}_{i1}\|^2 \\ & - \left(k_{\epsilon_{i2}} - \frac{1}{2}\right)\|\boldsymbol{\epsilon}_{i2}\|^2 + \frac{1}{2}\left\|\dot{\bar{\mathbf{Z}}}_{i2d}\right\|^2 + \frac{1}{2}\left\|\dot{\bar{\mathbf{v}}}_{i2}\right\|^2\Bigg]. \end{aligned} \tag{76}$$

Under the condition of (74a), the term $\gamma_{i1}\overset{\sim}{\vec{\omega}}_i^{(5)\mathrm{T}}\vec{\omega}_i$ has the following property:

$$-\gamma_{i1}\overset{\sim}{\vec{\omega}}_i^{(5)\mathrm{T}}\vec{\omega}_i^{(5)} \le \bar{\gamma}_{i1}\left(\bar{\omega}^{(5)} + 2\left\|\vec{\omega}^{(5)*}\right\|^2 - \frac{1}{2}\left\|\overset{\sim}{\vec{\omega}}_i^{(5)}\right\|^2\right). \quad (77)$$

The reason is as follows:

When $\bar{\omega}^{(5)} \ge \|\vec{\omega}_i^{(5)}\|^2$, $\gamma_{i1} = 0$, then

$$\begin{aligned}
-\gamma_{i1}\overset{\sim}{\vec{\omega}}_i^{(5)\mathrm{T}}\vec{\omega}_i^{(5)} = 0 &\le \bar{\gamma}_{i1}\left(\bar{\omega}^{(5)} - \left\|\vec{\omega}_i^{(5)}\right\|^2\right) \\
&= \bar{\gamma}_{i1}\left(\bar{\omega}^{(5)} - \left\|\vec{\omega}_i^{(5)*} + \overset{\sim}{\vec{\omega}}_i^{(5)*}\right\|^2\right) \\
&\le \bar{\gamma}_{i1}\left(\bar{\omega}^{(5)} - \left\|\left|\vec{\omega}_i^{(5)*}\right| - \left|\overset{\sim}{\vec{\omega}}_i^{(5)*}\right|\right\|^2\right) \\
&\le \bar{\gamma}_{i1}\left(\bar{\omega}^{(5)} + 2\left|\vec{\omega}_i^{(5)*}\right|^{\mathrm{T}}\left|\overset{\sim}{\vec{\omega}}_i^{(5)*}\right| - \left\|\overset{\sim}{\vec{\omega}}_i^{(5)*}\right\|^2\right) \\
&\le \bar{\gamma}_{i1}\left(\bar{\omega}^{(5)} + 2\left\|\vec{\omega}_i^{(5)*}\right\|^2 - \frac{1}{2}\left\|\overset{\sim}{\vec{\omega}}_i^{(5)*}\right\|^2\right).
\end{aligned} \quad (78)$$

On the other hand, when $\bar{\omega}^{(5)} < \|\vec{\omega}_i^{(5)}\|^2$, $\gamma_{i1} = \bar{\gamma}_{i1}$, then,

$$\begin{aligned}
-\gamma_{i1}\overset{\sim}{\vec{\omega}}_i^{(5)\mathrm{T}}\vec{\omega}_i^{(5)} &= -\bar{\gamma}_{i1}\overset{\sim}{\vec{\omega}}_i^{(5)\mathrm{T}}\left(\vec{\omega}_i^{(5)*} + \overset{\sim}{\vec{\omega}}_i^{(5)}\right) \\
&\le -\frac{1}{2}\bar{\gamma}_{i1}\left(\left\|\overset{\sim}{\vec{\omega}}_i^{(5)\mathrm{T}}\right\|^2 - \left\|\vec{\omega}_i^{(5)*}\right\|^2\right).
\end{aligned} \quad (79)$$

Hence, by combining (78) and (79), one can obtain (77). By the same way, one can conclude that

$$\begin{cases}
-\gamma_{i2}\tilde{\mathbf{c}}_i^T\mathbf{c}_i \le \bar{\gamma}_{i2}\left(\bar{c} + 2\|\boldsymbol{c}^*\|^2 - \frac{1}{2}\|\tilde{\boldsymbol{c}}_i\|^2\right), \\
-\gamma_{i3}\tilde{\boldsymbol{\sigma}}_i^T\boldsymbol{\sigma}_i \le \bar{\gamma}_{i3}\left(\bar{\sigma} + 2\|\boldsymbol{\sigma}^*\|^2 - \frac{1}{2}\|\tilde{\boldsymbol{\sigma}}_i\|^2\right), \\
-\gamma_{i4}\tilde{\boldsymbol{\omega}}_i^{F\mathrm{T}}\boldsymbol{\omega}_i^F \le \bar{\gamma}_{i4}\left(\bar{\omega}^F + 2\left\|\boldsymbol{\omega}^{F*}\right\|^2 - \frac{1}{2}\left\|\tilde{\boldsymbol{\omega}}_i^F\right\|^2\right), \\
-\gamma_{i5}\tilde{\boldsymbol{\omega}}_i^{rT}\boldsymbol{\omega}_i^r \le \bar{\gamma}_{i5}\left(\bar{\omega}^r + 2\|\boldsymbol{\omega}^{r*}\|^2 - \frac{1}{2}\|\tilde{\boldsymbol{\omega}}_i^r\|^2\right).
\end{cases} \quad (80)$$

Furthermore, the term $\gamma_{i6}\tilde{\mathbf{H}}_i^T\hat{\mathbf{H}}_i$ in (76) satisfies that

$$-\gamma_{i6}\tilde{\mathbf{H}}_i^{\mathrm{T}}\hat{\mathbf{H}}_i \le -\frac{1}{2}\gamma_{i6}\left(\left\|\tilde{\mathbf{H}}_i\right\|^2 - \|\mathbf{H}_i\|^2\right). \quad (81)$$

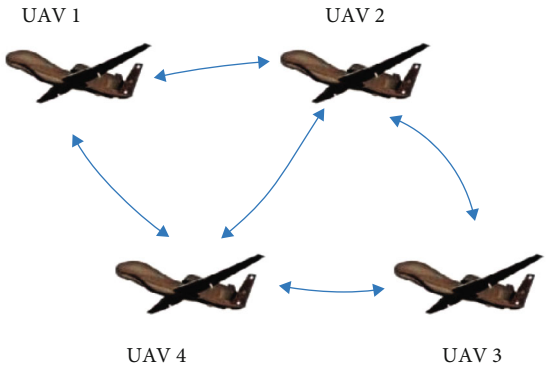

Figure 3: Communication topology.

Table 1: Initial attitudes of all UAVs.

	$\mu_i(0)$ (rad)	$\alpha_i(0)$ (rad)	$\beta_i(0)$ (rad)
UAV 1	0.01	0.01	0.01
UAV 2	-0.015	-0.015	-0.015
UAV 3	0.02	0.02	0.02
UAV 4	-0.025	-0.025	-0.025

Substituting (76) with (77), (80), and (81) then yeilds

$$\begin{aligned}
\dot{V} \le \sum_{i=1}^{N}\Bigg[&-\mathbf{E}_{i1}^{\mathrm{T}}\left(\mathbf{K}_{i1} - \frac{1}{2h_{i1}}\|A_i\mathbf{g}_{i1}(\mathbf{X}_{i1})\mathbf{G}_{i1}\|^2\right)\cdot\mathbf{E}_{i1} - \mathbf{E}_{i2}^{\mathrm{T}} \\
&\cdot\left(\mathbf{K}_{i2} - \frac{1}{2h_{i2}}\|\mathbf{g}_{i2}(\mathbf{X}_{i2})\mathbf{G}_{i20}\|^2\right)\mathbf{E}_{i2} - \mathbf{E}_{i3}^{\mathrm{T}}\mathbf{K}_{i3}\mathbf{E}_{i3}\Bigg] \\
&+ \sum_{i=1}^{N}\Bigg[-\frac{1}{2}\bar{\gamma}_{i1}\left\|\overset{\sim}{\vec{\omega}}_i^{(5)}\right\|^2 - \frac{1}{2}\bar{\gamma}_{i2}\cdot\|\tilde{\mathbf{c}}_i\|^2 - \frac{1}{2}\bar{\gamma}_{i3}\|\tilde{\boldsymbol{\sigma}}_i\|^2 \\
&- \frac{1}{2}\bar{\gamma}_{i4}\left\|\tilde{\boldsymbol{\omega}}_i^F\right\|^2 - \frac{1}{2}\bar{\gamma}_{i5}\cdot\|\tilde{\boldsymbol{\omega}}_i^r\|^2 - \frac{1}{2}\gamma_{i6}\left\|\tilde{\mathbf{H}}_i\right\|^2 \\
&- \left(k_{\epsilon_{i1}} - \frac{1+h_{i1}}{2}\right)\cdot\|\boldsymbol{\epsilon}_{i1}\|^2 - \left(k_{\boldsymbol{\epsilon}_{i2}} - \frac{1+h_{i2}}{2}\right)\|\boldsymbol{\epsilon}_{i2}\|^2\Bigg] + \delta,
\end{aligned} \quad (82)$$

where δ is

$$\begin{aligned}
\delta = \sum_{i=1}^{N}\Bigg[&\frac{1}{2}\left\|\dot{\bar{\mathbf{Z}}}_{i2d}\right\|^2 + \frac{1}{2}\left\|\dot{\bar{\mathbf{v}}}_{i2}\right\|^2 + \bar{\gamma}_{i1}\left(\bar{\omega}^{(5)} + 2\left\|\vec{\omega}^{(5)*}\right\|^2\right) \\
&+ \bar{\gamma}_{i2}\left(\bar{c} + 2\|\mathbf{c}^*\|^2\right) + \bar{\gamma}_{i3}\left(\bar{\sigma} + 2\|\boldsymbol{\sigma}^*\|^2\right) \\
&+ \bar{\gamma}_{i4}\left(\bar{\omega}^F + 2\left\|\boldsymbol{\omega}^{F*}\right\|^2\right) + \bar{\gamma}_{i5}\left(\bar{\omega}^r + 2\|\boldsymbol{\omega}^{r*}\|^2\right) + \frac{1}{2}\gamma_{i6}\|\mathbf{H}_i\|^2\Bigg].
\end{aligned} \quad (83)$$

By choosing the parameters $\mathbf{K}_{i1}$ and $\mathbf{K}_{i2}$ as

$$\begin{cases}
\mathbf{K}_{i1} = \mathbf{K}_{i10} + \frac{1}{2h_{i1}}\|A_i\mathbf{g}_{i1}(\mathbf{X}_{i1})\mathbf{G}_{i1}\|^2 \\
\mathbf{K}_{i2} = \mathbf{K}_{i20} + \frac{1}{2h_{i2}}\|\mathbf{g}_{i2}(\mathbf{X}_{i2})\mathbf{G}_{i20}\|^2
\end{cases}, \quad (84)$$

respectively, where $\mathbf{K}_{i10}$ and $\mathbf{K}_{i20}$ are positive diagonal

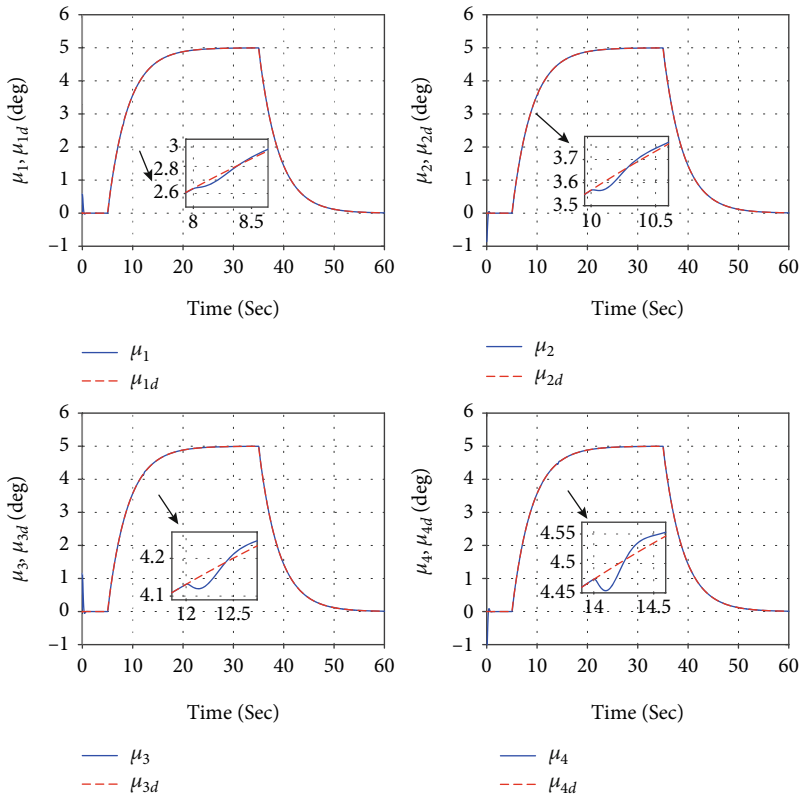

Figure 4: Bank angles μ_i and references μ_{id} of all UAVs ($i = 1, 2, 3, 4$).

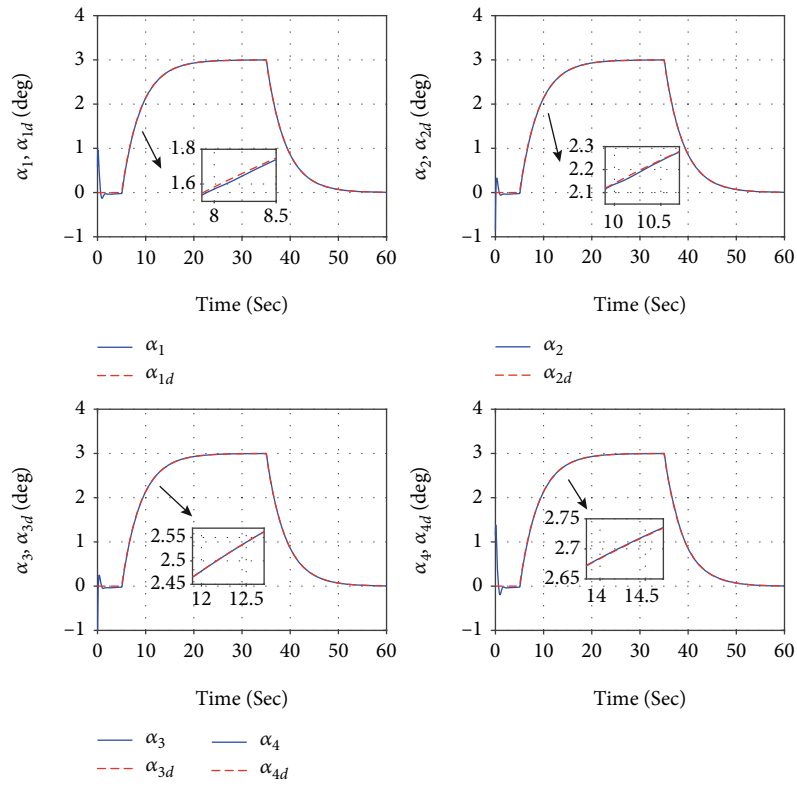

Figure 5: Attack angles α_i and references α_{id} of all UAVs ($i = 1, 2, 3, 4$).

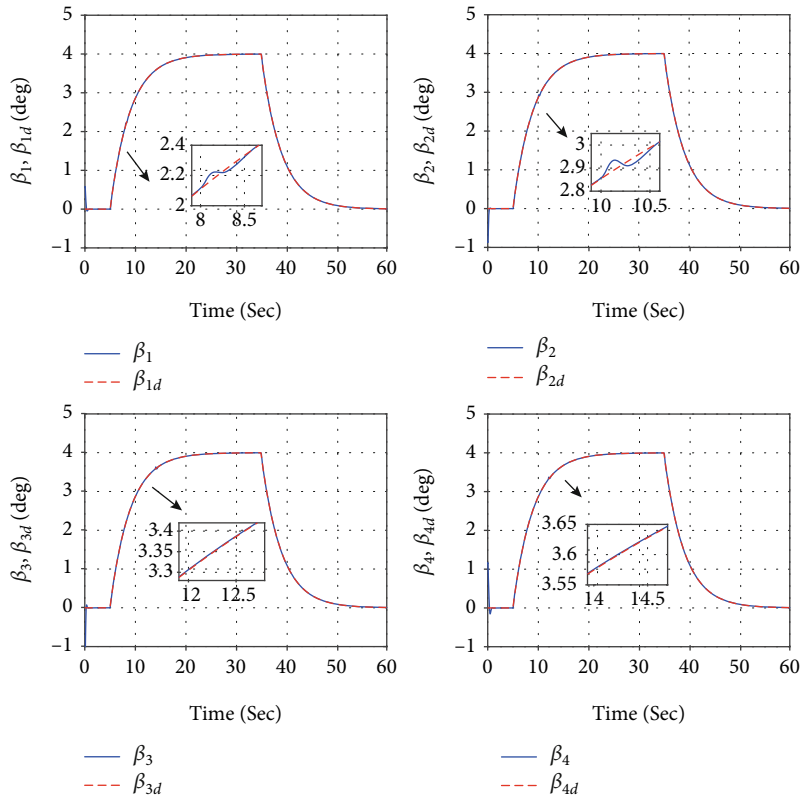

FIGURE 6: Sideslip angles β_i and references β_{id} of all UAVs ($i = 1, 2, 3, 4$).

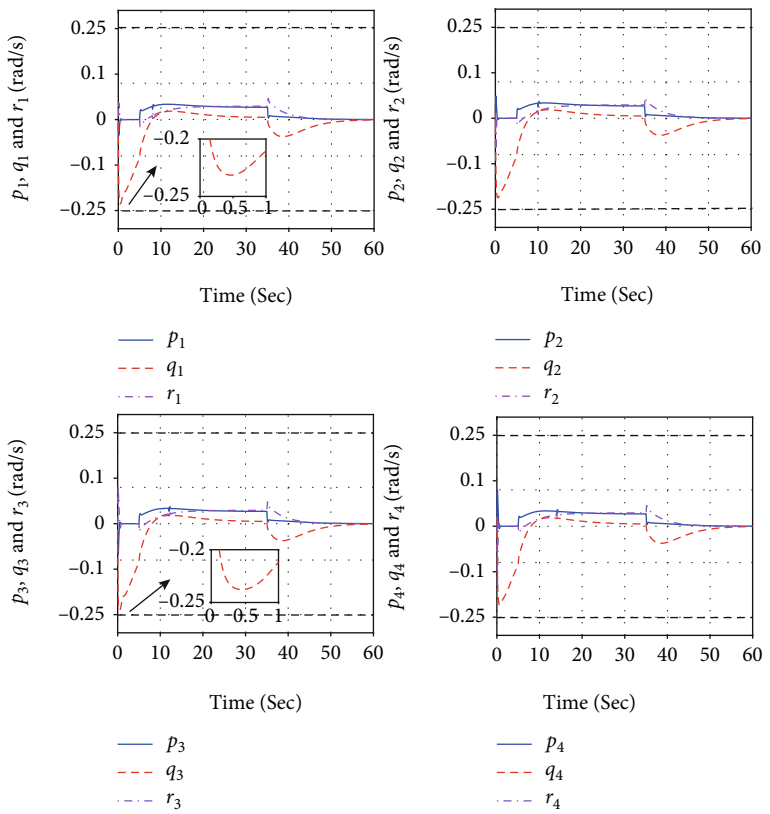

FIGURE 7: The time responses of p_i, q_i, and r_i with the developed control scheme ($i = 1, 2, 3, 4$).

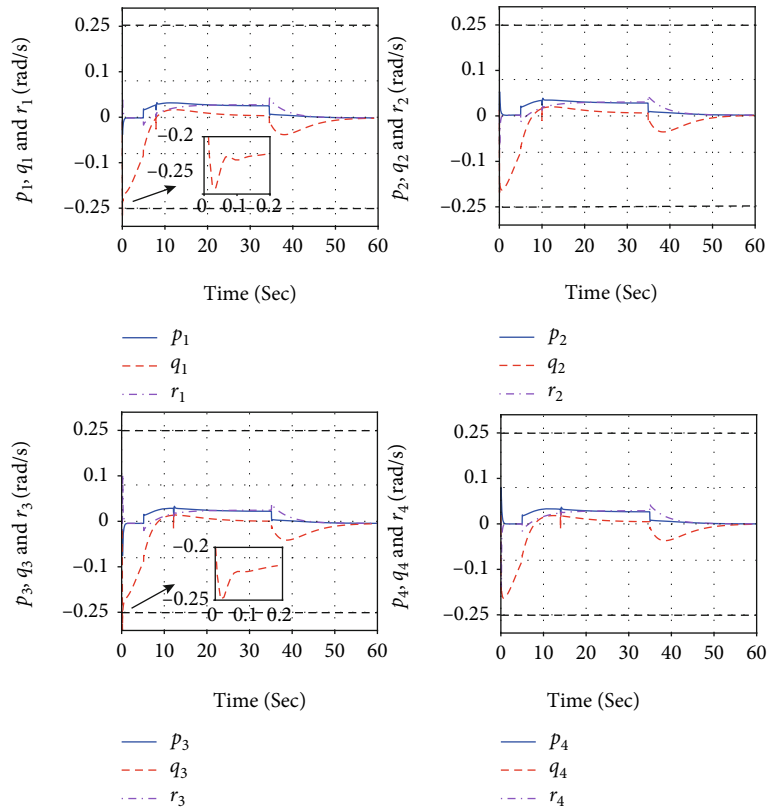

Figure 8: The time responses of p_i, q_i, and r_i without the constraint mechanism ($i = 1, 2, 3, 4$).

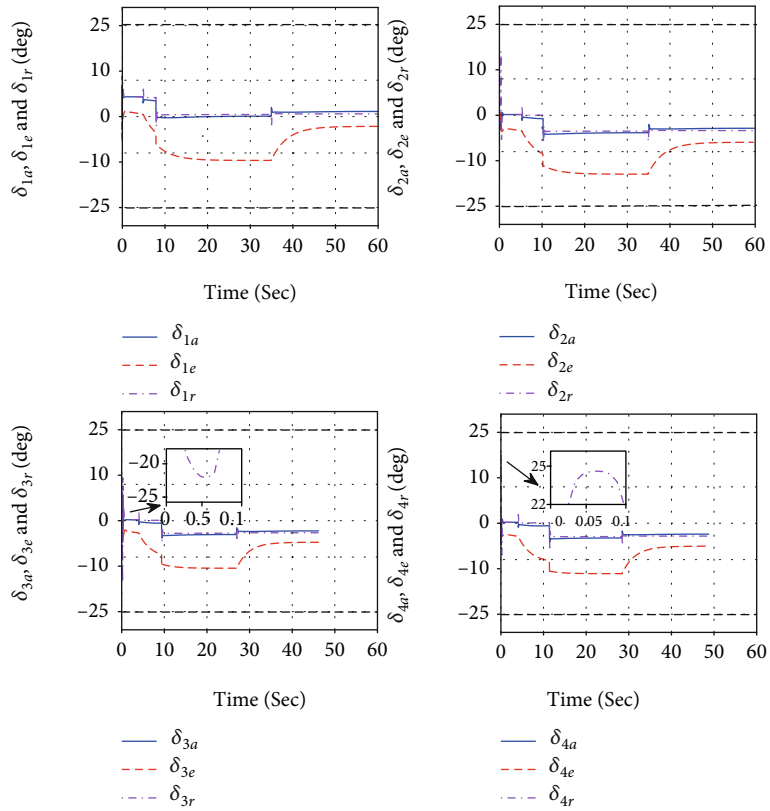

Figure 9: Control input signals δ_{ia}, δ_{ie}, and δ_{ir} of each UAVs ($i = 1, 2, 3, 4$).

matrices, (82) can be expressed as

$$\dot{V} \le -cV + \delta, \tag{85}$$

where c is

$$\begin{aligned} c = \min\{&\lambda_{\min}(2\mathbf{K}_{i10}), \lambda_{\min}(2\mathbf{K}_{i20}), \lambda_{\min}(2\mathbf{K}_{i30}), \\ &\eta_{i1}^{-1}\bar{\gamma}_{i1}, \eta_{i2}^{-1}\bar{\gamma}_{i2}, \eta_{i3}^{-1}\bar{\gamma}_{i3}, \eta_{i4}^{-1}\bar{\gamma}_{i4}, \eta_{i5}^{-1}\bar{\gamma}_{i5}, \eta_{i6}^{-1}\bar{\gamma}_{i6}, 2k_{\epsilon_{i1}} \\ &- 1 - h_{i1}, 2k_{\epsilon_{i2}} - 1 - h_{i2}\}. \end{aligned} \tag{86}$$

The expressions $\dot{\bar{\mathbf{Z}}}_{i2d}$ and $\dot{\bar{\mathbf{v}}}_{id}$ can be respectively obtained from (30) and (67), given by

$$\begin{aligned} \dot{\bar{\mathbf{Z}}}_{i2d} = &\frac{\partial \bar{\mathbf{Z}}_{i2d}}{\partial \mathbf{X}_{i1}}\dot{\mathbf{X}}_{i1} + \frac{\partial \bar{\mathbf{Z}}_{i2d}}{\partial \mathbf{E}_{i1}}\dot{\mathbf{E}}_{i1} + \frac{\partial \bar{\mathbf{Z}}_{i2d}}{\partial \mathbf{X}_{i1d}}\dot{\mathbf{X}}_{i1d} + \frac{\partial \bar{\mathbf{Z}}_{i2d}}{\partial \dot{\mathbf{X}}_{i1d}}\ddot{\mathbf{X}}_{i1d} \\ &+ \sum_{j\in N_i}^{j\neq i} a_{ij}\frac{\partial \bar{\mathbf{Z}}_{i2d}}{\partial \mathbf{Z}_{j1}}\dot{\mathbf{Z}}_{j1} + \frac{\partial \bar{\mathbf{Z}}_{i2d}}{\partial \mathbf{X}_{i2}}\dot{\mathbf{X}}_{i2} + \frac{\partial \bar{\mathbf{Z}}_{i2d}}{\partial \mathbf{Z}_{i2}}\dot{\mathbf{Z}}_{i2}, \\ \dot{\bar{\mathbf{v}}}_{id} = &\frac{\partial \bar{\mathbf{v}}_{id}}{\partial \mathbf{X}_{i1}}\dot{\mathbf{X}}_{i1} + \frac{\partial \bar{\mathbf{v}}_{id}}{\partial \mathbf{X}_{i2}}\dot{\mathbf{X}}_{i2} + \frac{\partial \bar{\mathbf{v}}_{id}}{\partial \mathbf{v}_i}\dot{\mathbf{v}}_i + \frac{\partial \bar{\mathbf{v}}_{id}}{\partial \hat{\mathbf{D}}_i}\dot{\hat{\mathbf{D}}}_i + \frac{\partial \bar{\mathbf{v}}_{id}}{\partial \hat{\Delta}_i}\dot{\hat{\Delta}}_i \\ &+ \frac{\partial \bar{\mathbf{v}}_{id}}{\partial \hat{\mathbf{H}}_i}\dot{\hat{\mathbf{H}}}_i + \frac{\partial \bar{\mathbf{v}}_{id}}{\partial \dot{\mathbf{Z}}_{i2d}}\ddot{\mathbf{Z}}_{i2d} + \frac{\partial \bar{\mathbf{v}}_{id}}{\partial \mathbf{E}_{i1}}\dot{\mathbf{E}}_{i1} + \frac{\partial \bar{\mathbf{v}}_{id}}{\partial \mathbf{E}_{i2}}\dot{\mathbf{E}}_{i2}. \end{aligned} \tag{87}$$

Define the following two vectors $\mathbf{X}_d$ and $\mathbf{E}_d$

$$\begin{cases} \mathbf{X}_d = \mathrm{col}\{\mathbf{X}_{1d}, \cdots, \mathbf{X}_{id}, \cdots, \mathbf{X}_{Nd}\}, \\ \mathbf{X}_{id} = \mathrm{col}\{\mathbf{X}_{i1d}, \dot{\mathbf{X}}_{i1d}, \ddot{\mathbf{X}}_{i1d}\}, \\ \mathbf{E}_d = \mathrm{col}\{\mathbf{E}_{1d}, \cdots, \mathbf{E}_{id}, \cdots, \mathbf{E}_{Nd}\}, \\ \mathbf{E}_i = \mathrm{col}\{\mathbf{E}_{i1}, \mathbf{E}_{i2}, \mathbf{E}_{i3}\}. \end{cases} \tag{88}$$

For any constants $\bar{B}_{X_d} > 0$, $\bar{B}_E > 0$, the sets $\mathscr{X} \coloneqq \{\mathbf{X}_d : \|\mathbf{X}_d\|^2 \le \bar{B}_{X_d}\}$ and $\mathscr{E} \coloneqq \{\mathbf{E}_d : \|\mathbf{E}_d\|^2 \le \bar{B}_E\}$ are compact ones. Then, $\mathscr{P} \coloneqq \mathscr{X} \times \mathscr{E}$ is also compact. Due to the fact that $\dot{\bar{\mathbf{Z}}}_{i2d}$ and $\dot{\bar{\mathbf{v}}}_{id}$ both are continuous function, considering the continuous property, there exists a constant $\delta_M > 0$ when $\forall (\mathbf{X}_d, \mathbf{E}_d) \in \mathscr{P}$ such that

$$\left\|\dot{\bar{\mathbf{Z}}}_{i2d}\right\|^2 + \left\|\dot{\bar{\mathbf{v}}}_{id}\right\|^2 \le \delta_M. \tag{89}$$

Therefore, there exists a constant $\bar{\delta} > 0$ satisfying

$$\delta \le \bar{\delta}, \forall (\mathbf{X}_d, \mathbf{E}_d) \in \mathscr{P}. \tag{90}$$

For any constant $\bar{B}_E$, there exists several parameters and initial condition satisfying

$$V(0) \le \bar{\delta}/c < 2\bar{\delta}/c \le \bar{B}_E, \tag{91}$$

such that

$$V(t) \le \frac{\bar{\delta}}{c}, \forall t \ge 0, \tag{92}$$

and $\mathscr{E}$ is an invariant set.

The above result (92) can be approved by contradiction. Since the reference input $\mathbf{X}_d$ must be bounded, that leads to $\mathbf{X}_d \in \mathscr{X}$ on $\forall t \ge 0$. Assuming $\exists t_1$, $V(t_1) > \bar{\delta}/c$, due to V is a continuous function, considering the continuous property, there exists a moment t_0 such that $V(t_0) = \bar{\delta}/c$, $V(t_{0+}) > \bar{\delta}/c$. Noticing $\|\mathbf{E}_d\|^2 \le 2V$ in (75), there exists $\|\mathbf{E}_d(t_0)\|^2 \le 2\bar{\delta}/c$. Considering (91) yields $(\mathbf{X}_d(t_0), \mathbf{E}_d(t_0)) \in \mathscr{P}$, so $\delta(t_0) \le \bar{\delta}$. Moreover, by taking account of (85), one can derive $\dot{V}(t_0) \le -cV(t_0) + \delta(t_0) = -\bar{\delta} + \delta(t_0) \le 0$. Hence, that causes $V(t_{0+}) \le V(t_0)$, which leads contradiction. This completes the proof of (91). Furthermore, considering $\|\mathbf{E}_d\|^2 \le 2V$ and (92), (91), one can derive $\mathscr{E}$ is an invariant set.

Therefore, all the signals in the system are uniformly bounded, and the states $\mathbf{X}_{i1}$, $\mathbf{X}_{i2}$ are always within their constraints. □

4. Simulation Results and Analysis

To illustrate the effectiveness and the superiority of the proposed FTCC scheme in this paper, using MATLAB/Simulink to simulate four UAVs whose communication topology is shown in Figure 3.

Figure 3 shows the communication network, and the parameters of UAVs are referred to [28]. The element a_{ij} of the adjacency matrix $\mathscr{A}$ is defined as 1 if the link between ith UAV and jth UAV existed; otherwise, $a_{ij} = 0$. The initial attitudes of all UAVs are presented in Table 1, and the initial angular rates are defined opposite as values of attitudes. The initial values of V_i, χ_i, and γ_i of all UAVs are set as 30 m/s, 0.01 rad and 0.01 rad, respectively.

Assuming the safe range of the attitudes μ_i, α_i, and β_i of all UAVs are $-8 \sim 8$ deg, and the corresponding angular velocity p_i, q_i, r_i are $-0.25 \sim 0.25$ rad/s. In addition, the maximum operation range of control surfaces δ_{ia}, δ_{ie}, and δ_{ir} are $-25 \sim 25$ deg.

Therefore, for any ith UAV, the upper bound $\bar{\mathbf{X}}_{i1}$ and the lower bound $\underline{\mathbf{X}}_{i1}$ of states $\mathbf{X}_{i1}$ are defined as $[8, 8, 8]^T$ deg and $-[8, 8, 8]^T$ deg, respectively. Similarly, the upper bound $\bar{\mathbf{X}}_{i2}$ and the lower bound $\underline{\mathbf{X}}_{i2}$ of states $\mathbf{X}_{i2}$ are $[0.25, 0.25, 0.25]^T$ rad/s and $-[0.25, 0.25, 0.25]^T$ rad/s, respectively. The upper bound $u_{i0\tau\ \max}$ and the lower bound $u_{i0\tau\ \min}$ are -25 deg and 25 deg, respectively.

The main control parameters are chosen as $\mathbf{K}_{i10} = \mathrm{diag}\{5, 5, 5\}$, $\mathbf{K}_{i20} = \mathrm{diag}\{20, 20, 20\}$, $\mathbf{K}_{i3} = \mathrm{diag}\{30, 30, 30\}$, $\eta_{i1} = \eta_{i2} = \eta_{i3} = \eta_{i4} = \eta_{i5} = 1.5$, $\eta_{i6} = 1.8$, $k_{\epsilon_{i1}} = k_{\epsilon_{i2}} = 100$, $h_{i1} = h_{i2} = 20$, and $\mu_{ib} = 0.001$.

To verify the effectiveness of the proposed FTCC scheme under actuator fault, the following fault signals are chosen:

$$\begin{cases} \boldsymbol{\rho}_1 = \boldsymbol{\rho}_2 = \boldsymbol{\rho}_3 = \boldsymbol{\rho}_4 = 1, \\ \mathbf{U}_{1f} = \mathbf{U}_{2f} = \mathbf{U}_{3f} = \mathbf{U}_{4f} = 0^\circ \end{cases} (t < 8)$$

$$\begin{cases} \boldsymbol{\rho}_1 = \text{diag}\,\{0.7,0.9,0.8\}, \\ \boldsymbol{\rho}_2 = \boldsymbol{\rho}_3 = \boldsymbol{\rho}_4 = 0, \\ \mathbf{U}_{1f} = [3^\circ, 2^\circ, 4^\circ]^T, \\ \mathbf{U}_{2f} = \mathbf{U}_{3f} = \mathbf{U}_{4f} = 0^\circ, \end{cases} (8 \le t < 10),$$

$$\begin{cases} \boldsymbol{\rho}_1 = \boldsymbol{\rho}_2\ \text{diag}\,\{0.7,0.9,0.8\}, \\ \boldsymbol{\rho}_3 = \boldsymbol{\rho}_4 = 0, \\ \mathbf{U}_{1f} = \mathbf{U}_{2f} = [3^\circ, 2^\circ, 4^\circ]^{\mathrm{T}}, \\ \mathbf{U}_{3f} = \mathbf{U}_{4f} = \mathbf{U}_{4f} = \mathbf{0}^\circ, \end{cases} (10 \le t < 12), \quad (93)$$

$$\begin{cases} \boldsymbol{\rho}_1 = \boldsymbol{\rho}_2 = \boldsymbol{\rho}_3 = \text{diag}\,\{0.7,0.9,0.8\}, \\ \boldsymbol{\rho}_4 = 0, \\ \mathbf{U}_{1f} = \mathbf{U}_{2f} = \mathbf{U}_{3f} = [3^\circ, 2^\circ, 4^\circ]^T, \\ \mathbf{U}_{4f} = 0^\circ, \end{cases} (12 \le t < 14),$$

$$\begin{cases} \boldsymbol{\rho}_1 = \boldsymbol{\rho}_2 = \boldsymbol{\rho}_3 = \boldsymbol{\rho}_4 = \text{diag}\,\{0.7,0.9,0.8\}, \\ \mathbf{U}_{1f} = \mathbf{U}_{2f} = \mathbf{U}_{3f} = \mathbf{U}_{4f} = [3^\circ, 2^\circ, 4^\circ]^T. \end{cases} (t \ge 14).$$

Remark 8. The reason of choosing the main control parameter briefly describes as follows. The parameter $\boldsymbol{K}_{i10}$ decides the closed-loop dynamics of $\dot{\boldsymbol{E}}_{i1}$, which can be approximated as $\dot{\boldsymbol{E}}_{i1} \approx -\boldsymbol{K}_{i1}\boldsymbol{E}_{i1} + \boldsymbol{E}_{i1}^T A_i g_{i1}(\boldsymbol{X}_{i1})\boldsymbol{G}_{i1}\boldsymbol{E}_{i2} + h_{i1}/2 \cdot \|\boldsymbol{\epsilon}_{i1}\|^2$ according to (32) and (84), and the term $\boldsymbol{E}_{i1}^T A_i g_{i1}(\boldsymbol{X}_{i1})\boldsymbol{G}_{i1}\boldsymbol{E}_{i2} + h_{i1}/2 \cdot \|\boldsymbol{\epsilon}_{i1}\|^2$will rapidly reduce due to the response of inner-loop dynamics $\boldsymbol{E}_{i2}$and $\boldsymbol{\epsilon}_{i1}$ are converge rapidly, then, it can be further represented as $\dot{\boldsymbol{E}}_{i1} \approx -\boldsymbol{K}_{i10}\boldsymbol{E}_{i1}$, so that the settling time of the dynamic $\boldsymbol{E}_{i1}$ approximately equal to $3/\lambda_{\min}(\boldsymbol{K}_{i10})$. There exists a tradeoff – a larger value $\boldsymbol{K}_{i10}$ helps to reduce the settling time while it needs larger change of the state $\boldsymbol{X}_{i2}$, which may cause saturation, so $\boldsymbol{K}_{i10}$ is taken as diag $\{5, 5, 5\}$. Similarly, parameters $\boldsymbol{K}_{i20}$ and $\boldsymbol{K}_{i3}$ decide the convergence rate of the inner-loop control errors $\boldsymbol{E}_{\mathrm{i2}}$ and $\boldsymbol{E}_{\mathrm{i3}}$, respectively, and their values normally take several times as the $\boldsymbol{K}_{\mathrm{i10}}$ to get faster response. Moreover, for parameters $\eta_{\mathrm{i1}} \sim \eta_{\mathrm{i6}}$, their inverses serve as learning rates of neural network, which usually take as a value among 1 ~ 1000 for fixed rate learning algorithms. In addition, parameters $k_{\epsilon_{\mathrm{i1}}}$ and $k_{\epsilon_{\mathrm{i2}}}$ are adjustment factors of dynamic surface filter, which are usually taken as a large value. Finally, for μ_{ib}, it can adjust the astringency of the error $\boldsymbol{E}_{\mathrm{i3}}$, which is the smaller the better, but the too small value will tend to cause virtual control signal "explosion".

The response of bank angle μ_i, angle of attack α_i, and sideslip angle β_i of each UAV are shown in Figures 4–6, respectively. It can be seen that all UAVs can track their references μ_{id}, α_{id}, and β_{id}. Although the fault occurs to UAV 1, UAV 2, UAV 3, and UAV 4 at 8 s, 10 s, 12 s, and 14 s, respectively, all UAVs can quickly track individual references again.

The response of state $\mathbf{X}_{i2}$ is shown in Figure 7. It can be seen that the states p_i, q_i, and r_i of all UAVs never exceed its upper or lower bound. Meanwhile, if the state constraints are not considered in the FTCC scheme, the states q_1 and q_3 will exceed the lower bound, which is shown in Figure 8. In addition, the control input signals δ_{ia}, δ_{ie}, and δ_{ir} are presented in Figure 9. Since the actuator constraint scheme (15) is adopted, the input signals never exceed their upper and lower bounds.

5. Conclusion and Future Work

This paper has explored an FTCC scheme for multi-UAVs under the distributed communication network, in which the issues including input saturation, state constraints, actuator faults, and unknown disturbances have all been taken into account.

It can be noted that the proposed FTCC scheme only considers fixed and undirected communication network. In addition, communication delay and communication interferences are not considered, and finite-time convergence technology has not been considered in the FTCC scheme, so the control performance cannot be achieved in finite time. Moreover, compared to the Euler attitude angles, the airflow attitude angles are necessary and easy to combine with the UAV's outer loop for position control, hence in this paper, it is directly used in the attitude control. However, using the airflow attitude angles for feedback control is less reliable than the former. Furthermore, sensor fault may occur at the same time, which perhaps outweigh the risk of actuator fault, so it deserves more attention and investigation. Finally, state measurements have been directly used in the control law without considering noise filtering, so that the performance may be degraded when sensor measurements have severe noises. Taking into account the noise filtering algorithms and sensor faults simultaneously will significantly increases the difficulty of proving the closed-loop system stability, which makes the issue challenging.

Therefore, in future work, the essence of communication delays, finite-time convergence technology, the reliability of using airflow attitude angle, sensor fault, and noise filtering will be taken into account on the basis of existing research. Besides, based on the simulation results from MATLAB/Simulink, the hardware-in-the-loop verification scheme will be adopted to further verify the proposed control scheme towards more practical applications.

Data Availability

No data were used to support this study.

Conflicts of Interest

The authors declare that they have no conflicts of interest.

Acknowledgments

This work was supported in part by National Natural Science Foundation of China (Nos. 61833013 and 62003162), Natural Science Foundation of Jiangsu Province of China (No. BK20200416), China Postdoctoral Science Foundation (Nos. 2020TQ0151 and 2020M681590), Aeronautical Science Foundation of China (No. 20200007018001), Science and Technology on Space Intelligent Control Laboratory (No. HTKJ2022KL502015), and Natural Sciences and Engineering Research Council of Canada.

References

[1] I. Bayezit and B. Fidan, "Distributed cohesive motion control of flight vehicle formations," *IEEE Transactions on Industrial Electronics*, vol. 60, no. 12, pp. 5763–5772, 2013.

[2] Y. Yang, H. Modares, K. G. Vamvoudakis, Y. Yin, and D. C. Wunsch, "Dynamic intermittent feedback design for H_∞ containment control on a directed graph," *IEEE Transactions on Cybernetics*, vol. 50, no. 8, pp. 3752–3765, 2019.

[3] A. Hegde and D. Ghose, "Multi-UAV collaborative transportation of payloads with obstacle avoidance," *IEEE Control Systems Letters*, vol. 6, pp. 926–931, 2022.

[4] X. Xiang, C. Liu, H. Su, and Q. Zhang, "On decentralized adaptive full-order sliding mode control of multiple UAVs," *ISA Transactions*, vol. 71, Part 2, pp. 196–205, 2017.

[5] K. Umemoto, T. Endo, and F. Matsuno, "Dynamic cooperative transportation control using friction forces of N multi-rotor unmanned aerial vehicles," *Journal of Intelligent & Robotic Systems*, vol. 100, no. 3-4, pp. 1085–1095, 2020.

[6] G. P. Kladis, P. P. Menon, and C. Edwards, "Fuzzy distributed cooperative tracking for a swarm of unmanned aerial vehicles with heterogeneous goals," *International Journal of Systems Science*, vol. 47, no. 16, pp. 3803–3811, 2016.

[7] L. He, X. Sun, and Y. Lin, "Distributed output-feedback formation tracking control for unmanned aerial vehicles," *International Journal of Systems Science*, vol. 47, no. 16, pp. 3919–3928, 2016.

[8] S. Park, J. Bae, Y. Kim, and S. Kim, "Fault tolerant flight control system for the tilt-rotor UAV," *Journal of the Franklin Institute*, vol. 350, no. 9, pp. 2535–2559, 2013.

[9] J. He, R. Qi, B. Jiang, and J. Qian, "Adaptive output feedback fault-tolerant control design for hypersonic flight vehicles," *Journal of the Franklin Institute*, vol. 352, no. 5, pp. 1811–1835, 2015.

[10] Z. Yu, Y. Zhang, B. Jiang, F. Jun, and Y. Jin, "A review on fault-tolerant cooperative control of multiple unmanned aerial vehicles," *Chinese Journal of Aeronautics*, vol. 35, no. 1, pp. 1–18, 2022.

[11] X. Qing, H. Yang, B. Jiang, D. Zhou, and Y. Zhang, "Fault tolerant formations control of UAVs subject to permanent and intermittent faults," *Journal of Intelligent & Robotic Systems*, vol. 73, no. 1-4, pp. 589–602, 2014.

[12] X. Yu, Z. Liu, and Y. Zhang, "Fault-tolerant formation control of multiple UAVs in the presence of actuator faults," *International Journal of Robust and Nonlinear Control*, vol. 26, no. 12, pp. 2668–2685, 2016.

[13] J. R. Azinheira and A. Moutinho, "Hover control of an UAV with backstepping design including input saturations," *IEEE Transactions on Control Systems Technology*, vol. 16, no. 3, pp. 517–526, 2008.

[14] S. Zhu and D. Wang, "Adversarial ground target tracking using UAVs with input constraints," *Journal of Intelligent & Robotic Systems*, vol. 65, no. 1-4, pp. 521–532, 2012.

[15] Y. Zhang, Y. Yang, Y. Zhao, and G. Wen, "Distributed finite-time tracking control for nonlinear multi-agent systems subject to external disturbances," *International Journal of Control*, vol. 86, no. 1, pp. 29–40, 2013.

[16] Z. Ding, "Consensus disturbance rejection with disturbance observers," *IEEE Transactions on Industrial Electronics*, vol. 62, no. 9, pp. 5829–5837, 2015.

[17] M. Chen, S. S. Ge, and B. Ren, "Adaptive tracking control of uncertain MIMO nonlinear systems with input constraints," *Automatica*, vol. 47, no. 3, pp. 452–465, 2011.

[18] J. Du, X. Hu, M. Krstić, and Y. Sun, "Robust dynamic positioning of ships with disturbances under input saturation," *Automatica*, vol. 73, pp. 207–214, 2016.

[19] B. Xu, "Disturbance observer-based dynamic surface control of transport aircraft with continuous heavy cargo airdrop," *IEEE Transactions on Systems, Man, and Cybernetics: Systems*, vol. 47, no. 1, pp. 161–170, 2017.

[20] Y. Yang, L. Tang, W. Zou, and D.-W. Ding, "Robust adaptive control of uncertain nonlinear systems with unmodeled dynamics using command filter," *International Journal of Robust and Nonlinear Control*, vol. 31, no. 16, pp. 7764–7784, 2021.

[21] Z. Yu, Y. Zhang, B. Jiang et al., "Composite adaptive disturbance observer-based decentralized fractional-order fault-tolerant control of networked UAVs," *IEEE Transactions on Systems, Man, and Cybernetics: Systems*, vol. 52, no. 2, pp. 799–813, 2022.

[22] Y. Yang and C. Z. Xu, "Adaptive fuzzy leader-follower synchronization of constrained heterogeneous multiagent systems," *IEEE Transactions on Fuzzy Systems*, vol. 30, no. 1, pp. 205–219, 2022.

[23] K. Zhao, L. Chen, and C. L. P. Chen, "Event-based adaptive neural control of nonlinear systems with deferred constraint," *IEEE Transactions on Systems, Man, and Cybernetics: Systems*, no. article 3143359, pp. 1–10, 2022.

[24] H. Bang, J. Kim, and Y. Jung, "Spacecraft attitude control compensating internal payload motion using disturbance observer technique," *International Journal of Aeronautical and Space Sciences*, vol. 20, no. 2, pp. 459–466, 2019.

[25] W. Qi, G. Zong, and S. F. Su, "Fault detection for semi-Markov switching systems in the presence of positivity constraints," *IEEE Transactions on Cybernetics*, 2021.

[26] W. Qi, G. Zong, and W. X. Zheng, "Adaptive event-triggered SMC for stochastic switching systems with semi-Markov process and application to boost converter circuit model," *IEEE Transactions on Circuits and Systems I: Regular Papers*, vol. 68, no. 2, pp. 786–796, 2021.

[27] H. He, W. Qi, Z. Liu, and M. Wang, "Adaptive attack-resilient control for Markov jump system with additive attacks," *Nonlinear Dynamics*, vol. 103, no. 2, pp. 1585–1598, 2021.

[28] Z. Yu, Y. Zhang, Z. Liu, Y. Qu, and C. Y. Su, "Distributed adaptive fractional-order fault-tolerant cooperative control of networked unmanned aerial vehicles via fuzzy neural networks," *IET Control Theory & Applications*, vol. 13, no. 17, pp. 2917–2929, 2019.

[29] J. D. Boskovic, S. E. Bergstrom, and R. K. Mehra, "Robust integrated flight control design under failures, damage, and state-dependent disturbances," *Journal of Guidance, Control, and Dynamics*, vol. 28, no. 5, pp. 902–917, 2005.

[30] K. Zhao, L. Chen, W. Meng, and L. Zhao, "Unified mapping function-based neuroadaptive control of constrained uncertain robotic systems," *Cybernetics*, vol. PP, pp. 1–10, 2022.

[31] K. Zhao, Y. Song, C. L. W. Meng, C. L. P. Chen, and L. Chen, "Low-cost approximation-based adaptive tracking control of output-constrained nonlinear systems," *IEEE Transactions on Neural Networks and Learning Systems*, vol. 32, no. 11, pp. 4890–4900, 2021.

[32] Z. Qu, "Matrix theory for cooperative systems," *Cooperative Control of Dynamical Systems: Applications to Autonomous Vehicles*, pp. 153–193, 2009.

[33] Z. Yu, Y. Zhang, B. Jiang et al., "Fractional-order adaptive fault-tolerant synchronization tracking control of networked fixed-wing UAVs against actuator-sensor faults via intelligent learning mechanism," *IEEE Transactions on Neural Networks and Learning Systems*, vol. 32, no. 12, pp. 5539–5553, 2021.